International Journal of Solids and Structures 51 (2014) 2878–2892

Contents lists available at ScienceDirect

International Journal of Solids and Structures

journal homepage: www.elsevier.com/locate/ijsolstr

# Development of a distributed dislocation dipole technique for the analysis of multiple straight, kinked and branched cracks in an elastic half-plane

N. Hallbäck *, M.W. Tofique

*Department of Engineering and Physics, Karlstad University, 65188 Karlstad, Sweden*

ARTICLE INFO

*Article history:*
Received 27 November 2013
Received in revised form 28 March 2014
Available online 24 April 2014

*Keywords:*
Cracks
Dislocation dipoles
Stress intensity factors
Singular integral equations

ABSTRACT

A distributed dislocation dipole technique for the analysis of multiple straight, kinked and branched cracks in an elastic half plane has been developed. The dipole density distribution is represented with a weighted Jacobi polynomial expansion where the weight function captures the asymptotic behaviour at each end of the crack. To allow for opening and sliding at crack kinking and branching the dipole density representation contains conditional extra terms which fulfills the asymptotic behaviour at each endpoint. Several test cases involving straight, kinked and branched cracks have been analysed, and the results suggest that the accuracy of the method is within 1% provided that Jacobi polynomial expansions up to at least the sixth order are used. Adopting even higher order Jacobi polynomials yields improved accuracy. The method is compared to a simplified procedure suggested in the literature where stress singularities associated with corners at kinking or branching are neglected in the representation for the dipole density distribution. The comparison suggests that both procedures work, but that the current procedure is superior, in as much as the same accuracy is reached using substantially lower order polynomial expansions.



## 1. Introduction

In many fatigue and fracture assessment cases, particularly early stages of fatigue, defects and cracks are small compared to other dimensions of the body. When fatigue is an issue it is also well known that initiation and incipient growth of short cracks dominates the total life of the structure. In such cases it is unnecessary to solve for the stress and strain state in the entire domain, except for a small neighbourhood adjacent to the crack or defect. Hence, the Finite Element Method (FEM) is not ideally suited for such situations. Due to the relatively low level of loading required to initiate and propagate cracks it is also evident that the body will mainly behave linear elastic. This is particularly so in case of Very High Cycle Fatigue (VHCF) (Bathias, 1999). Taking these facts into consideration, the problem is thus ideally suited to be treated by some Boundary Element Method (BEM) approach. However the presence of cracks inflicts some difficulties in traditional BEM (Cruse, 1988) based on infinite plane fundamental solutions for the displacements, since the upper and lower crack surfaces of a crack coincide, leading to identical equations for collocation points taken on opposite positions along the crack. The so called Dual Boundary Element Method (DBEM, see Portela et al., 1992; Mi, 1996), where Traction Boundary Integral Equations (BIE's) are used in combination with Displacement BIE's along the crack, has been used to circumvent this anomality, but there are other alternatives.

One alternative is the Distributed Dislocation Technique (DDT) where the derivative of the relative opening and sliding displacements of the crack surfaces are represented by distributions of dislocations (Bilby and Eshelby, 1968), or the Distributed Dislocation Dipole Technique (DDDT) where the opening and sliding displacements are represented by dislocation dipoles (Korsunsky and Hills, 1995). Both methods are described in detail in Hills et al. (1996). Yet another, but related technique, is the Displacement Discontinuity Method (DDM) originally developed by Crouch (1976). This technique is based on the stresses and displacements that results at a point due to constant displacement discontinuities over a finite length line segment in the body. This technique has been further improved by introducing line segments with higher order variations of the displacement discontinuities (Shou and Crouch,

* Corresponding author. Tel.: +46 54 700 21 15.
*E-mail addresses:* nils.hallback@kau.se (N. Hallbäck), muhammad-waqas.tofique@kau.se (M.W. Tofique).

http://dx.doi.org/10.1016/j.ijsolstr.2014.04.011
0020-7683/

1995). When applied to crack problems all of the abovementioned methods are usually adapted, by use of weight functions or by special interpolation formulas for the crack tip elements, to capture the square root singular behaviour of the stresses at the tip of a crack. By doing so, the analyses of stress intensity factors for straight cracks (single or multiple) are most often proven to be very efficient and accurate.

Of special interrest here is therefore the analysis of stress intensity factors in cases of kinked and/or branched cracks. If the kink or branch is disposed in such a way that an inward-bounded corner is formed in the material the stress state becomes singular, whereof the symmetric part possess the strongest singularity, while the asymmetric part exhibits a weaker singularity. Most often, however, the stress singularity associated with crack kinking is neglected in the formulation of kinked (or branched) crack problems. Zang and Gudmundson (1988) adopts the DDT for the part of the BIE's taken along the cracks and argue that the strongest stress singularity should be used to represent the asymptotic behaviour at a kink. In their benchmark analysis, however, they assume regular kink behaviour. Regular behaviour at crack kinking is also assumed in the BEM developed by Wang and Chau (1997), in the DDDT developed by Denda and Dong (1999) and in Marji and Dehghani (2010) who used a higher order DDM for the analyses of kinked cracks. At the other extreme the stress singularity at crack kinking is taken into consideration by assigning an oversevere, crack tip singularity, at the kink. This approach was taken in the DDT developed by Yingzhi and Hills (1990). A DDT accounting for both the asymmetric and symmetric singularity at crack kinking was presented by Burton and Phoenix (2000), and was further refined by Yavuz et al. (2006). Their method enables accurate determination of both the stress intensity factors as well as the strength of the singularities at crack kinking. In both studies the ableness of the method was demonstrated on single, or multiple, kinked or branched cracks in an infinite plane. Apart from edge cracks, branched cracks with singular behaviour at the branch were also excluded in their sample calculations.

While several investigators have been devoted to the development of the DDT to analyse kinked and branched cracks, less efforts have been made to apply the DDDT. A direct comparison between the two methods by Hills et al. (1996), on straight edge and interior cracks in a half plane, reveals that the DDDT requires less degrees of freedom in comparison to the DDT in order to obtain the same accuracy. This is particularly pronounced for edge cracks, since the DDDT does not inflict any artificial constraints on the behaviour at the crack mouth as opposed to the DDT. Hence convergence is accelerated with the DDDT in those cases.

Encouraged by these facts the DDDT is adopted in this development. The development is carried out for 2D, but the method is in principal applicable in 3D as well, albeit considerably more involved. The aim of this document is to present the method in a unified, but yet detailed and comprehensive, manner covering all possible situations within the scope of the title of the document. Possible contact between the crack surfaces is however disregarded, whence the method applies only for cracks that stay fully open. Care is taken to account for the singular behaviour of the stress field at crack kinking and branching, and to assess the accuracy and efficiency of the procedure as compared to the simplified approach where stress singularities at crack kinking/branching is neglected, such as in procedures developed by Denda and Dong (1999) among others. As proposed by Zang and Gudmundson (1988) the stress singularity at crack kinking is here assumed to be completely governed by the strongest singularity at the kink, which of course is an approximation to the exact nature of the singularity at a corner. The herein presented method could be extended to the analysis of finite two dimensional bodies by using techniques similar to that presented in Dai (2002).

### 1.1. Problem definition

Multiple surface or interior cracks close, or remote, to a free surface of an infinite half plane are considered. The cracks may either be straight or possess multiple kinks and/or branches. The number of straight crack segments, either in the form of straight cracks, or as a part of kinked and/or branched cracks, are denoted by $N$. The inclination angle of each straight crack segment referred to the positive $x_1$-axis is denoted by $\theta_i$, where $i$ denotes the segment number (see Fig. 1). The center point of each crack segment referred to the global $(x_1, x_2)$ system is denoted by $(c_1^{(i)}, c_2^{(i)})$. This report focuses on the evaluation of the stress intensity factors at each crack tip. A brief description on how to evaluate the stress state at an arbitrary location in the body will also be given.

## 2. Method

The numerical procedure is based on the fact that the stress intensity factors due to a remotely applied stress field can be computed by applying equivalent stresses acting on the crack surfaces in an identical but otherwise unloaded body. This principle is known as Bueckner's principle (Bueckner, 1958) which states that the equivalent stresses are the opposite to the stresses that act along cutting planes (coincident to crack segments in the cracked body) in the equivalent uncracked body subjected to the remote stress field in question. The cracks will respond to the applied stresses by opening and sliding displacements between the opposing crack surfaces. These displacements are represented by unknown distributions of dislocation dipole densities along each crack segment. The unknown coefficients of the distributions are determined by requiring that the stress state along the crack segments should be fulfilled. The stress conditions are enforced at certain points (collocation points), which results in two coupled integral equations for each component of stress at each collocation point. In addition to the collocation equations there are also certain continuity equations that have to be fulfilled at crack kinking and branching. By choosing an appropriate number of collocation points, the collocation integral equations and the continuity constraints results in a linear equation system which could be solved to obtain the unknown dislocation dipole density distribution. Once the dislocation dipole density distribution is known the stress intensity factors, and the stress state at any point in the body, could be evaluated.

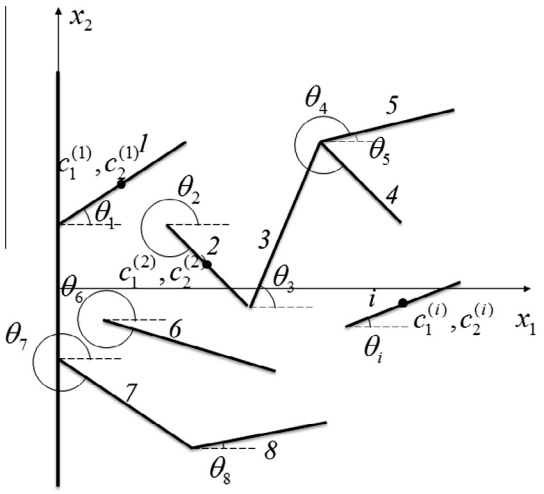


**Fig. 1.** Multiple straight, kinked and branched edge or internal cracks in a half plane.

### 2.1. Stresses due to dislocation dipoles

An infinitesimal dipole consists of two dislocations of opposite signs located an infinitesimal distance apart. Two dislocation dipoles, $b_{11}$ and $b_{21}$, corresponds to opening and sliding across the $x_2$ axis while the other two, $b_{22}$ and $b_{12}$, corresponds to opening and sliding across the $x_1$ axis, see Fig. 2(a). The stresses due to an arbitrary infinitesimal dislocation dipole could generally be expressed as Hills et al. (1996)

$$d\sigma_{ij} = \frac{2\mu}{\pi(\kappa+1)} db_{kl} L_{ij}^{kl} \tag{1}$$

where $L_{kl}^{ij}$ are dipole influence functions which depends on the geometry of the body, $\mu$ is the shear modulus and $\kappa = 3-4\nu$ for plane strain or $\kappa = (3-\nu)/(1+\nu)$ for plane stress. Note that superscripts are used to simplify notation, and not to indicate contravariant tensor components. A dislocation dipole equals the magnitude of the burgers vector of the dislocations times the distance between them. The dislocation dipole densities

$$B_{k1} = \frac{db_{k1}}{d\xi_2} \tag{2}$$

and

$$B_{k2} = \frac{db_{k2}}{d\xi_1} \tag{3}$$

are therefore equivalent to the opening and sliding of the material across the coordinate axis $x_2$ and $x_1$, respectively. In this report we consider cracks in an elastic half plane. Consider therefore a general infinitesimal dislocation dipole situated at $(\xi_1, \xi_2)$, referred to a cartesian coordinate system $(x_1, x_2)$, defined so that $x_1 = 0$ at the free surface (see Fig. 2(b)). The $L_{kl}^{ij}$ is preferably divided into two parts according to

$$L_{ij}^{kl} = \hat{L}_{ij}^{kl} + \bar{L}_{ij}^{kl} \tag{4}$$

where $\hat{L}_{ij}^{kl}$ and $\bar{L}_{ij}^{kl}$ are referred to as the singular and the regular part of $L_{ij}^{kl}$, respectively, due to reasons which will be obvious in later sections. The components for the singular and regular parts could be found in Hills et al. (1996). The singular part is a function of $\hat{x_1}$ and $\hat{x_2}$, *i.e.*

$$\hat{L}_{ij}^{kl} = \hat{L}_{ij}^{kl}(\hat{x}_1, \hat{x}_2) \tag{5}$$

while the regular part is a function of $\bar{x_1}$, $\bar{x_2}$ and $\xi_1$, so that

$$\bar{L}_{ij}^{kl} = \bar{L}_{ij}^{kl}(\bar{x}_1, \bar{x}_2, \xi_1) \tag{6}$$

### 2.2. Collocation integral equations

Suppose that the stress state is known for the equivalent uncracked body. For each crack $p$, with half cracklength $a_p$, a local coordinate system $(x_1^{(p)}, x_2^{(p)})$ is introduced at the center point of the crack $(c_1^{(p)}, c_2^{(p)})$, referred to the global $(x_1, x_2)$ system, so that the local $x_1^{(p)}$-axis is collinear with the crack. The normal and shear stresses acting along crack $p$ could then be expressed as

$$\begin{aligned} \bar{\sigma}_{22(p)}(x_1^{(p)}) &= -\tilde{\sigma}_{22(p)}(x_1^{(p)}) \\ \bar{\sigma}_{21(p)}(x_1^{(p)}) &= -\tilde{\sigma}_{21(p)}(x_1^{(p)}) \end{aligned} \tag{7}$$

where $\tilde{\sigma}_{22(p)}(x_1^{(p)})$ and $\tilde{\sigma}_{21(p)}(x_1^{(p)})$ are the stresses acting along the crack segment in the uncracked body. Subscript $ij(p)$ is here used to indicate that a tensor component $(ij)$ refers to the local coordinate system at crack segment $p$. To keep things simple two cracks ($q$ and $p$) are shown (see Fig. 3) in a body possibly containing many additional cracks (or crack segments). For each crack, say ($q$), dislocation dipoles corresponding to opening and sliding across the local coordinate axis $\xi_1^{(q)}$ are distributed. Due to Eq. (3) the relevant dislocation dipole components could be expressed as

$$db_{k2(q)}(\xi_1^{(q)}) = B_{k2(q)}(\xi_1^{(q)}) d\xi_1^{(q)}, \quad k = 1,2 \tag{8}$$

In order to apply Eq. (1), however, the local dislocation dipoles must be transformed to the global system. The infinitesimal dislocation dipole is a second rank tensor which transforms according to

$$db_{kl} = db_{mn(q)} \frac{\partial x_m^{(q)}}{\partial x_k} \frac{\partial x_n^{(q)}}{\partial x_l} \tag{9}$$

Adopting the following notation

$$\alpha_{mk}^{(q)} = \frac{\partial x_m^{(q)}}{\partial x_k} \tag{10}$$

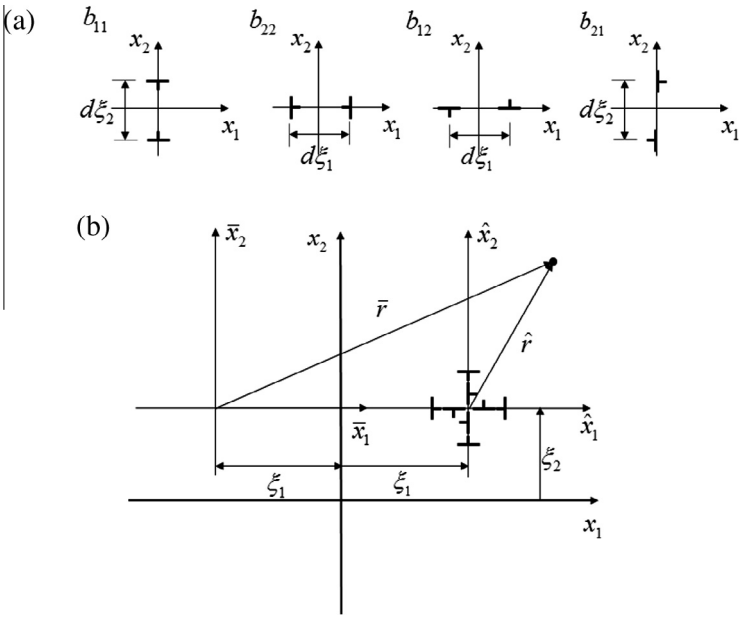


**Fig. 2.** (a) Dislocation dipoles and (b) a general dislocation dipole in an infinite half plane.

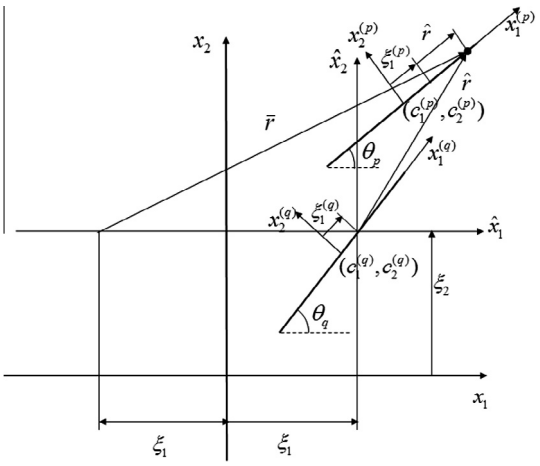


**Fig. 3.** Two cracks in an infinite half plane.

it is easily verified that the transformation matrix becomes

$$\alpha^{(q)} = \begin{bmatrix} \cos\theta_q & \sin\theta_q \\ -\sin\theta_q & \cos\theta_q \end{bmatrix} \tag{11}$$

Using this notation Eq. (9) reads as

$$db_{kl} = db_{mn(q)}\alpha_{mk}^{(q)}\alpha_{nl}^{(q)} \tag{12}$$

The stresses, referred to the global coordinate system, induced at any point on an arbitrary crack $p$ (including $q = p$), given by the coordinate $x_1^{(p)}$, due to the integrated effect from all distributed dislocation dipoles (*i.e* for all crack segments $q$), could by aid of Eqs. (1), (8) and (12), be expressed as

$$\bar{\sigma}_{ij}(x_1^{(p)}) = \frac{2\mu}{\pi(\kappa+1)}\sum_{q=1}^{N}\int_{-a_q}^{a_q} B_{m2}(\xi_1^{(q)})\alpha_{mk}^{(q)}\alpha_{2l}^{(q)}L_{ij}^{kl}(x_1^{(p)}, \xi_1^{(q)})d\xi_1^{(q)} \tag{13}$$

where $p = 1,\ldots N$ and $N$ is the total number of crack segments in the body. In order to apply the stress condition in Eq. (7), however, the stresses needs to be transformed to the local coordinate system at crack $p$. Since the inverse of $\alpha^{(q)}$ is equal to the transpose of $\alpha^{(q)}$, the stresses transforms as

$$\sigma_{rs(p)} = \alpha_{ri}^{(p)}\alpha_{sj}^{(p)}\sigma_{ij} \tag{14}$$

Inserting these transformations into Eq. (13), and invoking the stress condition in Eq. (7), gives the following expressions

$$\begin{aligned} -\tilde{\sigma}_{22(p)}(x_1^{(p)}) &= \frac{2\mu}{\pi(\kappa+1)}\sum_{q=1}^{N}\int_{-a_q}^{a_q} B_{m2(q)}(\xi_1^{(q)})\alpha_{2i}^{(p)}\alpha_{2j}^{(p)}\alpha_{mk}^{(q)}\alpha_{2l}^{(q)}L_{ij}^{kl}(x_1^{(p)}, \xi_1^{(q)})d\xi_1^{(q)} \\ -\tilde{\sigma}_{21(p)}(x_1^{(p)}) &= \frac{2\mu}{\pi(\kappa+1)}\sum_{q=1}^{N}\int_{-a_q}^{a_q} B_{m2(q)}(\xi_1^{(q)})\alpha_{2i}^{(p)}\alpha_{1j}^{(p)}\alpha_{mk}^{(q)}\alpha_{2l}^{(q)}L_{ij}^{kl}(x_1^{(p)}, \xi_1^{(q)})d\xi_1^{(q)} \end{aligned} \tag{15}$$

where $p = 1,\ldots N$. Introducing

$$L_{2g(p)}^{m2(q)} = \alpha_{2i}^{(p)}\alpha_{gj}^{(p)}\alpha_{mk}^{(q)}\alpha_{2l}^{(q)}L_{ij}^{kl} \tag{16}$$

where $L_{2g(p)}^{m2(q)}$ are dipole influence functions that relates the normal and shear stress components at $x_1^{(p)}$ at crack $p$ in the $x_1^{(p)}$, $x_2^{(p)}$ coordinate system to the relevant dislocation dipole density components at $\xi_1^{(q)}$ at crack $q$, expressed in the $x_1^{(q)}$, $x_2^{(q)}$ coordinate system. A detailed description of the transformation process is outlined in Appendix A. Using the above notation, Eqs. (15) could be expressed in compact form as

$$-\tilde{\sigma}_{2g(p)}(x_1^{(p)}) = \frac{2\mu}{\pi(\kappa+1)}\sum_{q=1}^{N}\int_{-a_q}^{a_q} B_{m2(q)}(\xi_1^{(q)})L_{2g(p)}^{m2(q)}(x_1^{(p)}, \xi_1^{(q)})d\xi_1^{(q)} \tag{17}$$

where $p = 1,\ldots N$, $g = 1,2$ and summation over repeated indices of $m = 1,2$ is understood.

The parameters needed to compute the components of the influence function in the above expression (see Eqs. (5) and (6)) are derived from $c_1^{(p)}$, $c_2^{(p)}$, $c_1^{(q)}$, $c_2^{(q)}$, $x_1^{(p)}$ and $\xi_1^{(q)}$ in the following way:

$$\begin{aligned} \hat{x}_1 &= c_1^{(p)} + x_1^{(p)}\cos\theta_p - \xi_1 \\ \hat{x}_2 &= c_2^{(p)} + x_1^{(p)}\sin\theta_p - \xi_2 \end{aligned} \tag{18}$$

where

$$\begin{aligned} \xi_1 &= c_1^{(q)} + \xi_1^{(q)}\cos\theta_q \\ \xi_2 &= c_2^{(q)} + \xi_1^{(q)}\sin\theta_q \end{aligned} \tag{19}$$

and

$$\begin{aligned} \bar{x}_1 &= 2\xi_1 + \hat{x}_1 \\ \bar{x}_2 &= \hat{x}_2 \end{aligned} \tag{20}$$

### 2.3. Scaling

In order to apply numerical integration techniques to solve the integral equation (Eq. (17)), it is convenient to introduce the following scalings

$$\begin{aligned} s &= \frac{\xi_1^{(q)}}{a_q} \\ t &= \frac{x_1^{(p)}}{a_p} \end{aligned} \tag{21}$$

so that $-1 < s < 1$ and $-1 < t < 1$. for the special case when $q = p$ the $\hat{L}$ part of $L$ equals

$$\hat{L}_{2g(p)}^{m2(p)}(x_1^{(p)}, \xi_1^{(p)}) = \hat{L}_{2g(p)}^{m2(p)}(t,s) = \frac{\delta_{gm}}{a_p^2(s-t)^2} \tag{22}$$

so that the integral equation (Eq. (17)) could be written as

$$\begin{aligned} -\frac{\pi(\kappa+1)}{2\mu}\tilde{\sigma}_{2g(p)}(t) = &\sum_{q=1,q\neq p}^{N} a_q\int_{-1}^{1} B_{m2(q)}(s)L_{2g(p)}^{m2(q)}(t,s)ds \\ &+\frac{1}{a_p}\int_{-1}^{1}\frac{B_{g2(p)}(s)}{(s-t)^2}ds + a_p\int_{-1}^{1} B_{m2(p)}(s)\bar{L}_{2g(p)}^{m2(p)}(t,s)ds \end{aligned} \tag{23}$$

where $p = 1,\ldots N$ and $g = 1,2$. When $s$ approaches $t$ it is seen that the integrand of the third term approaches infinity. The $\hat{L}$ is hence referred to as the singular part of $L$, while $\bar{L}$ is referred to as the regular part of $L$. In this case the singular part possess a hypersingular behaviour, which requires special treatment outlined in Section 2.6.

### 2.4. Corner elasticity

The stress state in the vicinity of a corner in an elastic body could be briefly expressed as Williams (1952).

$$\sigma_{ij} = \sum_{n=1}^{\infty} r^{\lambda_n^{(1)}-1}C_{n1}\Sigma_{n,ij}^{(1)}(\phi) + \sum_{n=1}^{\infty} r^{\lambda_n^{(2)}-1}C_{n2}\Sigma_{n,ij}^{(2)}(\phi) \tag{24}$$

where $r$ and $\phi$ are the coordinates of a polar coordinate system centered at the tip of the corner and $\Delta\theta$ is the angle occupied by the elastic material. The functions $\Sigma_{n,ij}^{(1)}(\phi)$ and $\Sigma_{n,ij}^{(2)}(\phi)$ corresponds to symmetric and asymmetric stress fields, respectively, with respect to the symmetry plane of the corner where $\phi = 0$. The eigenvalues corresponding to the symmetric and asymmetric modes are governed by

$$\begin{aligned}&\lambda^{(1)}\sin\Delta\theta+\sin\lambda^{(1)}\Delta\theta=0\\&-\lambda^{(2)}\sin\Delta\theta+\sin\lambda^{(2)}\Delta\theta=0\end{aligned}\tag{25}$$

The requirement that the strain energy must be bounded at the corner implies that only solutions for $\lambda$ greater than 0.5 are of interrest. Solving the above equations gives that the smallest values of interrest $0.5\leqslant\lambda_1^{(1)}\leqslant 1$ for $\pi\leqslant\Delta\theta\leqslant 2\pi$ and $0.5\leqslant\lambda_1^{(2)}\leqslant 1$ for $1.43\pi\leqslant\Delta\theta\leqslant 2\pi$, where $\lambda_1^{(1)}<\lambda_1^{(2)}$, except for a crack ($\Delta\theta=2\pi$) where both $\lambda_1^{(1)}=\lambda_1^{(2)}=0.5$. Hence, for a corner, the singularity associated with the symmetric part is stronger than the singularity governing the asymmetric part. For $0\leqslant\Delta\theta\leqslant\pi$ both $\lambda$ are equal or greater than one so that the stress state is always regular. In this work the asymptotic behaviour of the stresses at crack kinking or branching is assumed to behave according to the most singular part, i.e.

$$\sigma_{ij}\sim r^{\lambda_1^{(1)}-1}\tag{26}$$

whenever there is a corner angle such that $\Delta\theta>\pi$ at the kink or branch. This implies that the displacements along the free edges of the corner are assumed to behave as

$$u_i\sim r^{\lambda_1^{(1)}}\tag{27}$$

as $r\to 0$. This expression is used to specify the asymptotic behaviour of the crack opening and sliding displacements (and hence the dipole densities) close to an end point of a crack segment joined to another crack segment, at a kink or a branch, or terminating as a crack tip. This yields an exact representation for crack tips, but generally only an approximate treatment of the state at crack kinking. This is considered appropriate as long as the aim of the analysis is to compute the stress intensity factors, and not the details of the solution close to a kink or a branch forming a re-entrant corner into the material.

### 2.5. Dipole density representation

In order to solve for the dipole density distribution, the distribution has to be expressed in some suitable functional form. To capture arbitrary singular behaviour at each end point the dipole density distribution for any crack ($q$) is expressed by aid of a weight function $w^{(q)}(s)$ according to

$$\begin{aligned}B_{m2(q)}(s)=w^{(q)}(s)\phi_{m2}^{(q)}(s)+\bar{B}_{m2,+1}^{(q)}\frac{1}{2^{\gamma_-^{(q)}}}(1+s)^{\gamma_-^{(q)}}+\bar{B}_{m2,-1}^{(q)}\\\times\frac{1}{2^{\gamma_+^{(q)}}}(1-s)^{\gamma_+^{(q)}}\end{aligned}\tag{28}$$

where $\phi_{m2}^{(q)}(s)$ is a regular function and the weight function is

$$w^{(q)}(s)=(1-s)^{\gamma_+^{(q)}}(1+s)^{\gamma_-^{(q)}}\tag{29}$$

The first and second factors of the weight function should correspond to the behaviour of the dipole density at the positive (corresponding to $s=+1$) and the negative (corresponding to $s=-1$) end point, respectively, of the crack segment. The second and third terms in Eq. (28) are incorporated to account for opening and sliding of crack segment end points joined to a kink or branch. These extra terms are tailored to capture the asymptotic behaviour at the other end point of the crack segment, away from the kink or branch. For a kinked or branched crack the material locally bounded by two crack segments may occupy an angle $\Delta\theta>\pi$, in which case the end points of the crack segments involved behave weakly singular. The singularity is here taken to be governed by the smallest valid solution to the first of Eqs. (25), implying that $\gamma_+$ or $\gamma_-$, depending on which side of the crack segment that is part of the kink or branch, equals $\lambda_1^{(1)}$. If the angle ($\Delta\theta\leqslant\pi$) the exponent ($\gamma_+$ or $\gamma_-$) is set to zero to account for regular behaviour. This holds also for a crack reaching the free surface. If a crack segment end point, due to either reason, behaves regularly the corresponding extra term could be omitted. Practically this means that if $\gamma_+=0$, then $\bar{B}_{m2,+1}$ could be set to zero, and vice versa, since the regular behaviour then is accounted for solely by the first term of Eq. (28). The $\bar{B}_{m2,+1}$ (or $\bar{B}_{m2,-1}$) term could also be omitted if the corresponding end point of a crack segment ends as a crack tip, for which the exponent equals 1/2, since the opening and sliding displacements in such a case are zero. To sum up it is concluded that $\bar{B}_{m2,+1}$ and $\bar{B}_{m2,-1}$ could be expressed as

$$\begin{aligned}\bar{B}_{m2,+1}^{(q)}&=B_{m2,+1}^{(q)}\Delta(\gamma_+^{(q)})\\\bar{B}_{m2,-1}^{(q)}&=B_{m2,-1}^{(q)}\Delta(\gamma_-^{(q)})\end{aligned}\tag{30}$$

where the function $\Delta(\gamma)$ behaves as

$$\Delta(\gamma)=\begin{cases}0\text{ if }\gamma=0\vee\gamma=1/2\\1\text{ otherwise}\end{cases}\tag{31}$$

An example of a branched crack is given in Fig. 4, where the exponents associated with each crack segment end point are indicated in the figure. For each crack segment $q=1,\ldots N$ the regular function is expressed as a series of $N_p+1$ Jacobi polynomials with coefficients $c_{m2,n}^{(q)}$, where $m=1,2$ and $n=0,1,\ldots N_p$, *i.e.*

$$\phi_{m2}^{(q)}(s)=\sum_{n=0}^{N_p}c_{m2,n}^{(q)}P_n^{\gamma_+^{(q)},\gamma_-^{(q)}}(s)\tag{32}$$

where $\gamma_+^{(q)}$ and $\gamma_-^{(q)}$ denotes the exponents applicable for crack segment $q$. In the continuation of this paper, however, the shorter expression $P_n^{(q)}$ is used to denote $P_n^{\gamma_+^{(q)},\gamma_-^{(q)}}$. Hence

$$\begin{aligned}B_{m2(q)}(s)=(1-s)^{\gamma_+^{(q)}}(1+s)^{\gamma_-^{(q)}}\sum_{n=0}^{N_p}c_{m2,n}^{(q)}P_n^{(q)}(s)+\\B_{m2,+1}^{(q)}\Delta(\gamma_+^{(q)})\frac{1}{2^{\gamma_-^{(q)}}}(1+s)^{\gamma_-^{(q)}}+B_{m2,-1}^{(q)}\Delta(\gamma_-^{(q)})\frac{1}{2^{\gamma_+^{(q)}}}(1-s)^{\gamma_+^{(q)}}\end{aligned}\tag{33}$$

It is recognized that it would be possible to adopt different numbers of Jacobi polynomials for different crack segments, but here the same number of polynomials is used for all crack segments. Inserting the representation in Eq. (33) into the integral Eq. (23) yields

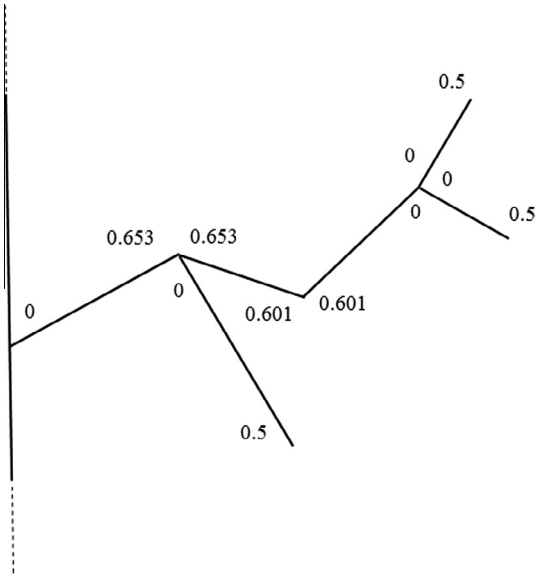


**Fig. 4.** End point singularities for a kinked and branched crack.

$$-\frac{\pi(\kappa+1)}{2\mu}\tilde{\sigma}_{2g}^{(p)}(t) = \sum_{q=1,q\neq p}^{N} a_q \left\{ \sum_{n=0}^{N_p} c_{m2,n}^{(q)} \int_{-1}^{1} (1-s)^{\gamma_+^{(q)}} (1+s)^{\gamma_-^{(q)}} P_n^{(q)}(s) L_{2g(p)}^{m2(q)}(t,s)ds + \frac{1}{2^{\gamma_-^{(q)}}} B_{m2,+1}^{(q)} \Delta(\gamma_+^{(q)}) \int_{-1}^{1} (1+s)^{\gamma_-^{(q)}} L_{2g(p)}^{m2(q)}(t,s)ds \right.$$
$$\left. + \frac{1}{2^{\gamma_+^{(q)}}} B_{m2,-1}^{(q)} \Delta(\gamma_-^{(q)}) \int_{-1}^{1} (1-s)^{\gamma_+^{(q)}} L_{2g(p)}^{m2(q)}(t,s)ds \right\}$$
$$+ \sum_{n=0}^{N_p} \left\{ \frac{c_{g2,n}^{(p)}}{a_p} \int_{-1}^{1} \frac{(1-s)^{\gamma_+^{(p)}} (1+s)^{\gamma_-^{(p)}} P_n^{(p)}(s)}{(s-t)^2} ds + a_p c_{m2,n}^{(p)} \int_{-1}^{1} (1-s)^{\gamma_+^{(p)}} (1+s)^{\gamma_-^{(p)}} P_n^{(p)}(s) \bar{L}_{2g(p)}^{m2(p)}(t,s)ds \right\}$$
$$+ \frac{B_{m2,+1}^{(p)} \Delta(\gamma_+^{(p)})}{2^{\gamma_-^{(p)}}} \left\{ \frac{\delta_{mg}}{a_p} \int_{-1}^{1} \frac{(1+s)^{\gamma_-^{(p)}}}{(s-t)^2} ds + a_p \int_{-1}^{1} (1+s)^{\gamma_-^{(p)}} \bar{L}_{2g(p)}^{m2(p)}(t,s)ds \right\}$$
$$+ \frac{B_{m2,-1}^{(p)} \Delta(\gamma_-^{(p)})}{2^{\gamma_+^{(p)}}} \left\{ \frac{\delta_{mg}}{a_p} \int_{-1}^{1} \frac{(1-s)^{\gamma_+^{(p)}}}{(s-t)^2} ds + a_p \int_{-1}^{1} (1-s)^{\gamma_+^{(p)}} \bar{L}_{2g(p)}^{m2(p)}(t,s)ds \right\} \quad p = 1,\ldots N,\ g = 1,2 \tag{34}$$

Evaluation of the integrals gives a linear equation system for the unknown dipole densities $c_{m2,n}^{(q)}$ and the end point displacements $B_{m2,-1}^{(q)}$ and $B_{m2,+1}^{(q)}$.

### 2.6. Computation of hypersingular integrals

The hypersingular integrals appearing in Eq. (34) should be interpreted in the Hadamard principal value (HPV) sense, which corresponds to the finite part of the hypersingular integral. Consider first the expression for the Cauchy principal value (CPV) of the singular integral (Kaya and Erdogan, 1987)

$$\int_{-1}^{1} \frac{(1-s)^{\gamma_+}(1+s)^{\gamma_-} P_n^{\gamma_+,\gamma_-}(s)}{(s-t)} ds = \pi \cot(\gamma_+\pi)(1-t)^{\gamma_+}(1+t)^{\gamma_-} P_n^{\gamma_+,\gamma_-}(t)$$
$$- \frac{2^{\gamma_++\gamma_-}\Gamma(\gamma_+)\Gamma(n+\gamma_-+1)}{\Gamma(n+\gamma_++\gamma_-+1)} F\left(n+1,-n-\gamma_+-\gamma_-,1-\gamma_+,\frac{1-t}{2}\right) \tag{35}$$

where $\Gamma$ denotes the gamma function, $F$ is the hypergeometric function and $P_n^{\gamma_+,\gamma_-}(s)$ is the Jacobi polynomial of order $n$. The above relation is valid for $\gamma_+,\ \gamma_- > -1$ and $\gamma_+ \neq 0,1,2,\ldots$. The Hadamard principal value of the hypersingular integral could be obtained by differentiating the Cauchy principal value of the corresponding singular integral (Kaya and Erdogan, 1987), *i.e.*

$$\oint_{-1}^{1} \frac{(1-s)^{\gamma_+}(1+s)^{\gamma_-} P_n^{\gamma_+,\gamma_-}(s)}{(s-t)^2} ds$$
$$= \frac{d}{dt} \int_{-1}^{1} \frac{(1-s)^{\gamma_+}(1+s)^{\gamma_-} P_n^{\gamma_+,\gamma_-}(s)}{(s-t)} ds$$
$$= -\pi \cot(\gamma_+\pi)\gamma_+(1-t)^{\gamma_+-1}(1+t)^{\gamma_-} P_n^{\gamma_+,\gamma_-}(t)$$
$$+ \pi \cot(\gamma_+\pi)(1-t)^{\gamma_+}\gamma_-(1+t)^{\gamma_--1} P_n^{\gamma_+,\gamma_-}(t)$$
$$+ \pi \cot(\gamma_+\pi)(1-t)^{\gamma_+}(1+t)^{\gamma_-} \frac{dP_n^{\gamma_+,\gamma_-}}{dt}(t)$$
$$+ \frac{2^{\gamma_++\gamma_--1}\Gamma(\gamma_+)\Gamma(n+\gamma_-+1)}{\Gamma(n+\gamma_++\gamma_-+1)} \frac{dF}{dt}\left(n+1,-n-\gamma_+-\gamma_-,1-\gamma_+,\frac{1-t}{2}\right)$$
$$= H_n\{\gamma_+,\gamma_-,t\} \tag{36}$$

where the derivative of the hypergeometric function could be computed from the hypergeometric function itself according to

$$\frac{dF}{dt}(a,b;c,t) = \frac{ab}{c} F(a+1,b+1;c+1,t) \tag{37}$$

and the derivative of the $n$th order Jacobi polynomial is obtained as

$$\frac{dP_n^{\gamma_+,\gamma_-}}{dt}(t) = \frac{1}{2}(n+\gamma_++\gamma_-+1) P_{n-1}^{\gamma_++1,\gamma_-+1}(t) \tag{38}$$

In Eq. (36) $H_n\{\gamma_+,\gamma_-,t\}$ is introduced to denote the hypersingular integral of the weighted Jacobi polynomial of order $n$. The case when $\gamma_+ = 0$, or when both $\gamma_+$ and $\gamma_-$ are zero obviously needs some special attention, since the above expression cannot be used right away in those cases. By laterally reversing the coordinate axis, by letting $s = -s'$ and $t = -t'$, and utilizing the symmetry relation for Jacobi polynomials, *i.e.*

$$P_n^{\gamma_+,\gamma_-}(-s) = (-1)^n P_n^{\gamma_-,\gamma_+}(s) \tag{39}$$

the HPV in Eq. (36) transforms into

$$\oint_{-1}^{1} \frac{(1-s)^{\gamma_+}(1+s)^{\gamma_-} P_n^{\gamma_+,\gamma_-}(s)}{(s-t)^2} ds = (-1)^n \oint_{-1}^{1} \frac{(1-s')^{\gamma_-}(1+s')^{\gamma_+} P_n^{\gamma_-,\gamma_+}(s')}{(s'-t')^2} ds' \tag{40}$$

which implies that the HPV when $\gamma_+ = 0$ could be evaluated as

$$H_n\{0,\gamma_-,t\} = (-1)^n H_n\{\gamma_-,0,-t\} \tag{41}$$

The case when $\gamma_+ = \gamma_- = 0$ is treated as Kaya and Erdogan (1987)

$$\oint_{-1}^{1} \frac{P_n^{0,0}(s)}{(s-t)^2} ds = -\frac{2(n+1)}{1-t^2}[tQ_n(t) - Q_{n+1}(t)] = H_n\{0,0,t\} \tag{42}$$

by virtue of the fact that $P_n^{0,0}$ corresponds to the Legendre polynomial of the same order. In the above expression $Q_n$ is the Legendre function of the second kind. Since $P_0^{\gamma_+,\gamma_-}(s) = 1$ The HPV's

$$\oint_{-1}^{1} \frac{(1+s)^{\gamma_-}}{(s-t)^2} ds = H_0\{0,\gamma_-,t\} = H_0\{\gamma_-,0,-t\} \tag{43}$$

and finally

$$\oint_{-1}^{1} \frac{(1-s)^{\gamma_+}}{(s-t)^2} ds = H_0\{\gamma_+,0,t\} \tag{44}$$

where again the $H$ function has been introduced to shorten the notation in subsequent expressions.

### 2.7. Computation of regular integrals

The regular integrals in Eq. (34) involving the weightening factor $(1-s)^{\gamma_+}(1+s)^{\gamma_-}$ multiplied by some smooth continuous function, which is here briefly denoted as $\psi(s)$, can be computed by applying the Gauss–Jacobi quadrature rule for integration of functions with that particular weight. The numerical integration could then be expressed as

$$\int_{-1}^{1}(1-s)^{\gamma_+}(1+s)^{\gamma_-}\psi(s)ds=\sum_{i=1}^{M}W_i^{\gamma_+,\gamma_-}\psi(s_i^{\gamma_+,\gamma_-}) \tag{45}$$

where the abscissas $s_i^{\gamma_+,\gamma_-}$ are the $M$ roots to the equation $P_M^{\gamma_+,\gamma_-}(s)=0$, and $W_i^{\gamma_+,\gamma_-}$ are the associated weights. By letting $\gamma_-=\gamma_+=0$ this expression also embodies the numerical integration of unweighted integrals. The numerical integration scheme is then referred to as Gauss–Legendre quadrature with abscissas $s_i^{0,0}$ and weights $W_i^{0,0}$. The abscissas, and their associated weights, can be obtained by standard procedures found in any textbook, or website, dealing with orthogonal polynomials.

### 2.8. Collocation procedure

The unknown coefficients in the dipole density representation for each crack segment $q$ and each $m$ ($m=1,2$) (cf. Eq. (33)) comprises $c_{m2,n}^{(q)}$ ($n=0,\dots N_p$) and one, or both, of the coefficients $B_{m2,+1}^{(q)}$ and $B_{m2,-1}^{(q)}$, depending on the value of $\gamma_+^{(q)}$ and $\gamma_-^{(q)}$. By letting $N_u^{(q)}$ denote the number of unknown coefficients for each $m$, and for each crack segment $q=1,\dots N$, the total number of unknown coefficients for each $m$ in Eq. (34) equals $N_u=\sum_{q=1}^{N}N_u^{(q)}$. At each branch or kink there will be two continuity equations for each $m$, one for the dipole densities and one for the derivative of the dipole densities (see Section 2.9). The number of collocation points for each crack is adapted to render the problem determinate, i.e. so that the total number of equations equals the number of unknown coefficients. To accomplish this, $N_p+1$ collocation points are initially allocated at each crack segment. If the problem is overdetermined the number of collocation points is first reduced by one on crack segments not bounded by a crack tip. If the problem is still overdetermined one collocation point is consecutively removed also from crack segments bounded by a crack tip, until the problem is determinate. The determinate problem will then adopt at least $N_c^{(p)}=N_p$ or at most $N_c^{(p)}=N_p+1$ collocation points for each crack segment, and the total number of collocation points is $N_c=\sum_{p=1}^{N}N_c^{(p)}$. The collocation point coordinates are choosen to coincide with the $N_c^{(p)}$ points along each crack segment where the Chebyshev polynomial of the first kind, of order $N_c^{(p)}$, is zero. The collocation point coordinates are hence given by

$$t_k^{(p)}=\cos\left(\frac{\pi}{2}\frac{2k-1}{N_c^{(p)}}\right),\quad k=1,2,\dots N_c^{(p)} \tag{46}$$

Using the numerical integration of the regular integrals as described in Section 2.7, and the expressions for the hypersingular integrals in Section 2.6 the integral Eq. (34) could be expressed as

$$\begin{aligned}-\frac{\pi(\kappa+1)}{2\mu}\tilde{\sigma}_{2g}^{(p)}(t_k^{(p)})=&\sum_{q=1,q\neq p}^{N}a_q\Bigg\{\sum_{n=0}^{N_p}c_{m2,n}^{(q)}\sum_{i=1}^{M}W_i^{(q)}P_n^{(q)}(s_i^{(q)})L_{2g(p)}^{m2(q)}\left(t_k^{(p)},s_i^{(q)}\right)+B_{m2,+1}^{(q)}\Delta(\gamma_+^{(q)})\frac{1}{2^{\gamma_-^{(q)}}}\sum_{i=1}^{M}W_i^{0,\gamma_-^{(q)}}L_{2g(p)}^{m2(q)}\left(t_k^{(p)},s_i^{0,\gamma_-^{(q)}}\right)\\&+B_{m2,-1}^{(q)}\Delta(\gamma_-^{(q)})\frac{1}{2^{\gamma_+^{(q)}}}\sum_{i=1}^{M}W_i^{\gamma_+^{(q)},0}L_{2g(p)}^{m2(q)}\left(t_k^{(p)},s_i^{\gamma_+^{(q)},0}\right)\Bigg\}\\&+\sum_{n=0}^{N_p}\Bigg\{\frac{c_{g2,n}^{(p)}}{a_p}H_n\{\gamma_+^{(p)},\gamma_-^{(p)},t_k^{(p)}\}+a_pc_{m2,n}^{(p)}\sum_{i=1}^{M}W_i^{(p)}P_n^{(p)}(s_i^{(p)})\bar{L}_{2g(p)}^{m2(p)}\left(t_k^{(p)},s_i^{(p)}\right)\Bigg\}\\&+\frac{B_{m2,+1}^{(p)}\Delta(\gamma_+^{(p)})}{2^{\gamma_-^{(p)}}}\Bigg\{\frac{\delta_{mg}}{a_p}H_0\{0,\gamma_-^{(p)},t_k^{(p)}\}+a_p\sum_{i=1}^{M}W_i^{0,\gamma_-^{(p)}}\bar{L}_{2g(p)}^{m2(p)}\left(t_k^{(p)},s_i^{0,\gamma_-^{(p)}}\right)\Bigg\}\\&+\frac{B_{m2,-1}^{(p)}\Delta(\gamma_-^{(p)})}{2^{\gamma_+^{(p)}}}\Bigg\{\frac{\delta_{mg}}{a_p}H_0\{\gamma_+^{(p)},0,t_k^{(p)}\}+a_p\sum_{i=1}^{M}W_i^{\gamma_+^{(p)},0}\bar{L}_{2g(p)}^{m2(p)}\left(t_k^{(p)},s_i^{\gamma_+^{(p)},0}\right)\Bigg\}\quad p=1,\dots,N,\ k=1,\dots,N_c^{(p)},\ g=1,2\end{aligned} \tag{47}$$

where the weights, $W_i^{(q)}=W_i^{\gamma_+^{(q)},\gamma_-^{(q)}}$, and the abscissas, $s_i^{(q)}=s_i^{\gamma_+^{(q)},\gamma_-^{(q)}}$, are computed for the particular $\gamma_+^{(q)}$ and $\gamma_-^{(q)}$ pertaining to crack segment $q$. Repeatedly applying Eq. (47) at each collocation point, and for each of the two stress components, results in a linear equation system in the following form

$$-\frac{\pi(\kappa+1)}{2\mu}\begin{bmatrix}\tilde{\sigma}_{22}^{(1)}(t_1)\\\vdots\\\tilde{\sigma}_{22}^{(1)}(t_{N_c^{(1)}})\\\tilde{\sigma}_{21}^{(1)}(t_1)\\\vdots\\\tilde{\sigma}_{21}^{(1)}(t_{N_c^{(1)}})\\\vdots\\\tilde{\sigma}_{22}^{(N)}(t_1)\\\vdots\\\tilde{\sigma}_{22}^{(N)}(t_{N_c^{(N)}})\\\tilde{\sigma}_{21}^{(N)}(t_1)\\\vdots\\\tilde{\sigma}_{21}^{(N)}(t_{N_c^{(N)}})\end{bmatrix}=\begin{bmatrix}\Lambda_{11}&\Lambda_{12}&\dots&\Lambda_{1,2N_u}\\\Lambda_{21}&\Lambda_{22}&\dots&\Lambda_{2,2N_u}\\\vdots&\vdots&\ddots&\vdots\\\Lambda_{2N_c,1}&\Lambda_{2N_c,2}&\dots&\Lambda_{2N_c,2N_u}\end{bmatrix}\begin{bmatrix}\zeta_{2,1}^{(1)}\\\vdots\\\zeta_{2,N_u^{(1)}}^{(1)}\\\zeta_{1,1}^{(1)}\\\vdots\\\zeta_{1,N_u^{(1)}}^{(1)}\\\vdots\\\zeta_{2,1}^{(N)}\\\vdots\\\zeta_{2,N_u^{(N)}}^{(N)}\\\zeta_{1,1}^{(N)}\\\vdots\\\zeta_{1,N_u^{(N)}}^{(N)}\end{bmatrix} \tag{48}$$

where the unknown coefficients for each crack segment, and for each $m$, are arranged in vectors according to

$$\begin{bmatrix} \zeta^{(q)}_{m,1} \\ \zeta^{(q)}_{m,2} \\ \vdots \\ \zeta^{(q)}_{m,N^{(q)}_u} \end{bmatrix} = \begin{bmatrix} c^{(q)}_{m2,0} \\ c^{(q)}_{m2,1} \\ \vdots \\ c^{(q)}_{m2,N_p} \\ B^{(q)}_{m2,+1}\Delta(\gamma^{(q)}_+) \\ B^{(q)}_{m2,-1}\Delta(\gamma^{(q)}_-) \end{bmatrix} \tag{49}$$

By virtue of the fact that it is unnecessary to treat $B_{m2,\pm1}$ coefficients which are multiplied by zero via the $\Delta(\gamma^{(q)}_\pm)$ function, the number $N^{(q)}_u$ is at least $N_p+1$ and at most $N_p+3$. In short notation Eq. (48) can be expressed as

$$S_r = \Lambda_{rs} C_s \tag{50}$$

For each crack $p = 1,\dots N$ the integral Eq. (47) is applied at all collocation points $t^{(p)}_k,\ k = 1,\dots N^{(p)}_c$, for each stress component $g = 1,2$. The components $\Lambda_{rs}$ are computed by integrating along all cracks $q = 1,\dots N$ the influence from each coefficient $\zeta^{(q)}_{m,n_u}$ $(n_u = 1,\dots N^{(q)}_u, m = 1,2)$ on the stress component under consideration. The indices $r$ and $s$ are derived from $p,\ q,\ g,\ m,\ k$ and $n_u$ as

$$\begin{aligned} r &= 2\sum_{i=1}^{p} N^{(i)}_c - gN^{(p)}_c + k \\ s &= 2\sum_{i=1}^{q} N^{(i)}_u - mN^{(q)}_u + n_u \end{aligned} \tag{51}$$

The components of the system matrix $\Lambda$ depends on whether $q = p$ or not, and on which coefficient that is considered in relation to the total number of coefficients for each crack segment. The following expressions for the components apply:

- if $n_u \leqslant N_p + 1$ then

$$\Lambda_{rs} = a_q \sum_{i=1}^{M} W^{(q)}_i P^{(q)}_n(s^{(q)}_i) L^{m2(q)}_{2g(p)}(t^{(p)}_k, s^{(q)}_i) \text{ if } q \neq p$$

$$\Lambda_{rs} = \frac{\delta_{mg}}{a_p} H_n\{\gamma^{(p)}_+, \gamma^{(p)}_-, t^{(p)}_k\} + a_p \sum_{i=1}^{M} W^{(p)}_i P^{(p)}_n(s^{(p)}_i) \bar{L}^{m2(p)}_{2g(p)}(t^{(p)}_k, s^{(p)}_i) \text{ if } q = p$$

where $n = n_u - 1$.

- if $n_u = N_p + 2 \wedge [\{N^{(q)}_u = N_p + 2 \wedge \Delta(\gamma^{(q)}_+) = 1\} \vee N^{(q)}_u = N_p + 3]$ then

$$\Lambda_{rs} = \frac{a_q}{2^{\gamma^{(q)}_-}} \sum_{i=1}^{M} W^{0,\gamma^{(q)}_-}_i L^{m2(q)}_{2g(p)}(t^{(p)}_k, s^{0,\gamma^{(q)}_-}_i) \text{ if } q \neq p$$

$$\Lambda_{rs} = \frac{\delta_{mg}}{2^{\gamma^{(p)}_-} a_p} H_0\{0, \gamma^{(p)}_-, t^{(p)}_k\} + \frac{a_p}{2^{\gamma^{(q)}_-}} \sum_{i=1}^{M} W^{0,\gamma^{(p)}_-}_i \bar{L}^{m2(p)}_{2g(p)}(t^{(p)}_k, s^{0,\gamma^{(p)}_-}_i) \text{ if } q = p$$

- if $\{n_u = N_p + 2 \wedge N^{(q)}_u = N_p + 2 \wedge \Delta(\gamma^{(q)}_-) = 1\} \vee n_u = N_p + 3$ then

$$\Lambda_{rs} = \frac{a_q}{2^{\gamma^{(q)}_+}} \sum_{i=1}^{M} W^{\gamma^{(q)}_+,0}_i L^{m2(q)}_{2g(p)}(t^{(p)}_k, s^{\gamma^{(q)}_+,0}_i) \text{ if } q \neq p$$

$$\Lambda_{rs} = \frac{\delta_{mg}}{2^{\gamma^{(p)}_+} a_p} H_0\{\gamma^{(p)}_+, 0, t^{(p)}_k\} + \frac{a_p}{2^{\gamma^{(p)}_+}} \sum_{i=1}^{M} W^{\gamma^{(p)}_+,0}_i \bar{L}^{m2(p)}_{2g(p)}(t^{(p)}_k, s^{\gamma^{(p)}_+,0}_i) \text{ if } q = p$$

Note that the hypersingular integrals only need to be computed once for all crack segments possessing the same end point behaviours and the same number of collocation points.

### 2.9. Continuity equations

At crack kinking and/or branching the net opening and sliding displacements (i.e the dislocation dipole densities) of the adjacent crack segments should cancel out. By letting $s \to \pm 1$, depending on whether it is the plus side or the minus side of the crack segment that is joined to a kink or a branch (subsequently referred to as a *node*), this condition could be expressed as

$$\sum_{q\in Q_i} \pm \alpha^{(q)}_{mk} B_{k2(q)}(s \to \pm 1) = 0 \tag{52}$$

In this equation $\alpha_{mk}$ is given by Eq. (11), and $Q_i$ denotes the set of all crack segments joined at node $i = 1,\dots,N_n$, where $N_n$ is the number of nodes in the model. The upper or the lower sign applies depending on if the plus side, or the minus side, of the particular crack segment $q$ connects to the node, respectively. Introducing the expression for the dipole density distribution (Eq. (33)) into Eq. (52) yields

$$\sum_{q\in Q_i} \pm \alpha^{(q)}_{mk} \left\{ \Psi(\gamma^{(q)}_\pm) 2^{\gamma^{(q)}_\mp} \sum_{n=0}^{N_p} c^{(q)}_{k2,n} P^{(q)}_n(\pm 1) B^{(q)}_{k2,\pm1} \Delta(\gamma^{(q)}_\pm) + B^{(q)}_{k2,\mp1} \Delta(\gamma^{(q)}_\mp) \Psi(\gamma^{(q)}_\pm) \right\} = 0 \tag{53}$$

where $\Psi(\gamma)$ behaves such that

$$\Psi(\gamma) = \begin{cases} 1 \text{ if } \gamma = 0 \\ 0 \text{ if } 0.5 < \gamma < 1 \end{cases} \tag{54}$$

Eq. (53) yields two equations (corresponding to $m = 1,2$). Taking the derivative of Eq. (52) ensures compatible rotations of the crack segment end points at the node. According to Hills et al. (1996) this condition preserves continuity of the dislocation density at crack kinking or branching. *Viz.*

$$\sum_{q\in Q_i} \pm \alpha^{(q)}_{mk} \frac{1}{a_q} \frac{dB_{k2(q)}}{ds}(s \to \pm 1) = 0 \tag{55}$$

Invoking the representation for the dipole density distribution (Eq. (33)) gives

$$\begin{aligned} \sum_{q\in Q_i} \Bigg[ & \frac{-1}{(1-|s\to\pm1|)^{1-\gamma^{(q)}_\pm}} \frac{\alpha^{(q)}_{mk}}{a_q} \left\{ \gamma^{(q)}_\pm 2^{\gamma^{(q)}_\mp} \sum_{n=0}^{N_p} c^{(q)}_{k2,n} P^{(q)}_n(\pm1) + B^{(q)}_{k2,\mp1} \Delta(\gamma^{(q)}_\mp) \frac{\gamma^{(q)}_\pm}{2^{\gamma^{(q)}_\pm}} \right\} \\ & + (\pm) \frac{\alpha^{(q)}_{mk}}{a_q} \Psi(\gamma^{(q)}_\pm) 2^{\gamma^{(q)}_\pm} \left\{ \pm \sum_{n=0}^{N_p} c^{(q)}_{k2,n} P^{(q)}_n(\pm1) + \sum_{n=0}^{N_p} c^{(q)}_{k2,n} \frac{dP^{(q)}_n}{ds}(\pm1) \right\} \\ & + \frac{\alpha^{(q)}_{mk}}{a_q} B^{(q)}_{k2,\pm1} \Delta(\gamma^{(q)}_\pm) \frac{\gamma^{(q)}_\mp}{2} \Bigg] = 0 \end{aligned} \tag{56}$$

where the first term obviously turns to infinity whenever there are any two crack segments meeting at a node so that the material locally bounded by the crack segments occupies an angle $\Delta\theta > \pi$. The exponents capturing the singularity at the node are then equal (for both crack segments $0.5 < \gamma^{(q)}_\pm < 1$), implying that the strength of the singular term for such crack segments in Eq. (56) are equal. In such cases the remaining terms are clearly negigible, and Eq. (56) is asymptotically satisfied if

$$\sum_{q\in Q_i} \frac{\alpha^{(q)}_{mk}}{a_q} \left\{ \gamma^{(q)}_\pm 2^{\gamma^{(q)}_\mp} \sum_{n=0}^{N_p} c^{(q)}_{k2,n} P^{(q)}_n(\pm1) + B^{(q)}_{k2,\mp1} \Delta(\gamma^{(q)}_\mp) \frac{\gamma^{(q)}_\pm}{2^{\gamma^{(q)}_\pm}} \right\} = 0 \tag{57}$$

where $\hat{Q}_i$ is the subset $Q_i$ containing crack segments with weakly singular end point behaviour at node $i$. The number of crack segments contained in $\hat{Q}_i$ is either zero or two, i.e.

$$|\hat{Q}_i| = 0 \vee 2 \tag{58}$$

If $|\hat{Q}_i| = 0$ all crack segment end points behave regularly at the node, implying that $\gamma_{\pm}^{(q)} = 0$. The singular term of Eq. (56) then vanish, and the remaining regular terms must obey the relationship

$$\sum_{q\in Q_i}\left[(\pm)\frac{\alpha_{mk}^{(q)}}{a_q}\Psi(\gamma_{\pm}^{(q)})2^{\gamma_{\mp}^{(q)}}\left\{\pm\sum_{n=0}^{N_p}c_{k2,n}^{(q)}P_n^{(q)}(\pm1)+\sum_{n=0}^{N_p}c_{k2,n}^{(q)}\frac{dP_n^{(q)}}{ds}(\pm1)\right\}+\frac{\alpha_{mk}^{(q)}}{a_q}B_{k2,\pm1}^{(q)}\Delta(\gamma_{\pm}^{(q)})\frac{\gamma_{\mp}^{(q)}}{2}\right]=0 \tag{59}$$

### 2.10. Computation of the dipole density coefficients

As previously stated the number of collocation points is adapted to render the problem determinate. The linear equation system, given by the collocation procedure and the continuity constraints, is solved by gaussian elimination. Once the coefficients of the dipole density distributions for every crack segment (Eq. (33)) are known, the stress intensity factors and the stress state at any arbitrary location in the half plane could be evaluated.

### 2.11. Stress intensity factor evaluation

The inplane stress intensity factors $K_I$ and $K_{II}$ are the strengths of the symmetric and asymmetric parts, respectively, of the singular part of the stress field close to a crack tip. With this notation the singular part of the stress field could be expressed as

$$\sigma_{ij} = \frac{K_I}{\sqrt{2\pi r}}\bar{\Sigma}_{ij}^{(I)}(\phi)+\frac{K_{II}}{\sqrt{2\pi r}}\bar{\Sigma}_{ij}^{(II)}(\phi) \tag{60}$$

where $\bar{\Sigma}_{ij}^{(I)}$ and $\bar{\Sigma}_{ij}^{(II)}$ essentially corresponds to $\Sigma_{1,ij}^{(1)}$ and $\Sigma_{1,ij}^{(2)}$ in Eq. (24) when $\Delta\theta = 2\pi$, though somewhat rescaled. The functions $\bar{\Sigma}_{ij}^{(I)}(\phi)$ and $\bar{\Sigma}_{ij}^{(II)}(\phi)$ are well known and can be found in any textbook on fracture mechanics. The symmetry properties imply that the term involving $K_I$ corresponds to opening of the crack tip, while the term involving $K_{II}$ corresponds to sliding. By aid of Hookes generalized law these stresses can be integrated to obtain the corresponding displacements and, hence, the relative crack surface opening and sliding displacements as $r \to 0$. The result is

$$\Delta u_2 = \frac{\kappa+1}{\mu}K_I\sqrt{\frac{r}{2\pi}} \qquad \Delta u_1 = \frac{\kappa+1}{\mu}K_{II}\sqrt{\frac{r}{2\pi}} \tag{61}$$

where $\Delta u_2$ is the opening displacement and $\Delta u_1$ is the sliding displacement. Close to the crack tip the displacements given by Eq. (61) should asymptotically conform to the dipole density distributions $B_{22}$ and $B_{12}$, respectively. Each end point of a crack segment which is a sharp crack tip will be associated to a pair of stress intensity factors. For a crack tip located at either the plus side ($t = +1$), or the minus side ($t = -1$), the stress intensity factors could be derived as

$$\begin{aligned}K_I^{(q)}(t=\pm1) &= \lim_{t\to\pm1}\frac{2\mu}{(\kappa+1)}\sqrt{\frac{\pi}{2a_q(1\mp t)}}B_{22(q)}(t)\\ K_{II}^{(q)}(t=\pm1) &= \lim_{t\to\pm1}\frac{2\mu}{(\kappa+1)}\sqrt{\frac{\pi}{2a_q(1\mp t)}}B_{12(q)}(t)\end{aligned} \tag{62}$$

where $q$ refers to the crack segment that accommodates the crack tip. Introducing the representation for the dipole density distributions (Eq. (33)) the above expressions transmogrify into

$$\begin{aligned}\frac{K_I^{(q)}(t=\pm1)}{\sqrt{\pi a_q}} &= \frac{\mu}{a_q(\kappa+1)}\left\{2^{\gamma_{\mp}^{(q)}+1/2}\sum_{n=0}^{N_p}c_{22,n}^{(q)}P_n^{(q)}(\pm1)+B_{22,\mp1}^{(q)}\Delta(\gamma_{\mp}^{(q)})\right\}\\ \frac{K_{II}^{(q)}(t=\pm1)}{\sqrt{\pi a_q}} &= \frac{\mu}{a_q(\kappa+1)}\left\{2^{\gamma_{\mp}^{(q)}+1/2}\sum_{n=0}^{N_p}c_{12,n}^{(q)}P_n^{(q)}(\pm1)+B_{12,\mp1}^{(q)}\Delta(\gamma_{\mp}^{(q)})\right\}\end{aligned} \tag{63}$$

### 2.12. Stress analysis at an arbitrary field point

Analysing the stress state at an arbitray location in the half-plane, away from the cracks, could be done by again considering the superposition principle (Bueckner's principle, see Section 2). The stress state in the cracked body is given by the stress state in the uncracked body $\tilde{\sigma}_{kl}$ plus the stresses that results from applying the equivalent stress state along the crack segments in the cracked body without any remote loading (see Section 2). The stress state is hence given by

$$\sigma_{kl}(x_j) = \tilde{\sigma}_{kl}(x_j)+\hat{\sigma}_{kl}(x_j) \tag{64}$$

where $\sigma_{kl}(x_j)$ is the stress state at the arbitrary location of interrest and $x_j$ is the location expressed in the global coordinate system. The latter stress state $\hat{\sigma}_{kl}(x_j)$ is given by the integrated effect from the dislocation dipole distributions along each crack segment in the half plane. Hence, the $\hat{\sigma}_{kl}(x_j)$ stress state is essentially derived using Eq. (13). In that equation the transformation of the influence functions relevant for the computation of stresses expressed in the global system $x_j$ due to dipole densities expressed in the local system $x_j^{(q)}$ appears as (with a change of indices)

$$L_{kl}^{m2(q)} = \alpha_{mr}^{(q)}\alpha_{2s}^{(q)}L_{kl}^{rs} \tag{65}$$

A detailed description of this transformation is given in Appendix A. Inserting Eq. (65), the dipole density distribution and the scaling into Eq. (13), and finally employing numerical integration, yields the expression for the stresses as

$$\sigma_{kl}(x_j) = \tilde{\sigma}_{kl}(x_j)+\frac{2\mu}{\pi(\kappa+1)}\sum_{q=1}^{N}a_q\left\{\sum_{n=0}^{N_p}c_{m2,n}^{(q)}\sum_{i=1}^{M}W_i^{(q)}P_n^{(q)}(s_i^{(q)})L_{kl}^{m2(q)}(x_j,s_i^{(q)})+B_{m2,+1}^{(q)}\Delta(\gamma_+^{(q)})\frac{1}{2^{\gamma_-^{(q)}}}\sum_{i=1}^{M}W_i^{0,\gamma_-^{(q)}}L_{kl}^{m2(q)}(x_j,s_i^{0,\gamma_-^{(q)}})+B_{m2,-1}^{(q)}\Delta(\gamma_-^{(q)})\frac{1}{2^{\gamma_+^{(q)}}}\sum_{i=1}^{M}W_i^{\gamma_+^{(q)},0}L_{kl}^{m2(q)}(x_j,s_i^{\gamma_+^{(q)},0})\right\} \tag{66}$$

Provided that the field point is not located along a crack segment it is observed that none of the integrals involved will be singular. Hence all integrals can be treated by regular integration as described in Section 2.7.

### 2.13. Numerical implementation

The method is currently implemented in Matlab. An object oriented technique is adopted to accommodate variables associated with each crack segment. Variables which potentially may appear several times in the analysis are evaluated before the main computation loop, and stored in arrays for subsequent use.

### 2.14. Example problems

Some example problems are analysed in order to verify the accuracy of the method, and to assure that the implementation is

done correctly. The stress intensity factors obtained with the present DDDT are compared to the stress intensity factors obtained by aid of the FEM, using the multipurpose FE-code ABAQUS. The example problems under consideration are.

(a) A single kinked edge crack
(b) Multiple edge and internal cracks
(c) A kinked internal crack
(d) A doubly kinked internal crack
(e) A branched internal crack
(f) A kinked and branched internal crack
(g) A doubly branched internal crack
(h) A branched internal crack with a weak singularity at the branch

Cases (a) to (d) are shown in Fig. 5, and cases (e) to (h) are shown in Fig. 6. The single kinked edge crack is analysed for several different combinations of the kink angle ($\varphi = 30^\circ$, $55^\circ$ and $80^\circ$) and the kink length ($a_2/a_1 = 0.2$, 0.1 and 0.05), where $a_1$ was set to 10 mm. In the second case (b) $a_1 = 6$ mm, $a_2 = 8$ mm, $a_1 = 10$ mm, $l_2 = 9$ mm, $l_3 = 7$ mm and $h_2 = 2$ mm. In the remaining cases $a_1 = 10$ mm, $a_2 = 3$ mm and $l_1 = 5$ mm. The loading consists in all cases of a remotely applied unixal stress $\sigma_{yy\infty} = 100$ MPa in the global $y$-direction. The encircled numbers in Figs. 5 and 6 indicate the crack tip number, which is referred to in Tables 1–11.

### 2.15. FE-analysis

In order to mimic an elastic half plane the cracks were located close to the vertical free surface of a rectangular region with width and height typically 1000 times the typical crack length. The horisontal boundaries were subjected to the uniform tensile stress $\sigma_{yy\infty}$. Each crack tip were modelled with a surrounding focussed mesh with 32 elements circumferentially and 10 elements radially. Eight-noded biquadratic elements where used where the crack tip elements were collapsed to a single node at the crack tip and the mid sides nodes at the radial element edges where moved to the so-called quarter point position to emulate the square root singular behaviour of the stresses. An example of a mesh used is depicted in Fig. 7, which shows the deformed mesh of case (h). The stress intensity factors where computed for 10 contours around the crack tip by aid of the built in domain integration technique in ABAQUS. Since the variation in the results for the outermost contours were very small the results presented in Tables 1–11 apply for any contour between the 5th and 10th contour within the given accuracy. The finite element procedure was tested by analysing a 120° V-shaped crack in an infinite domain subjected to uniform tension. The results for the stress intensity factors differed by less than 0.04% compared to the results reported by Burton and Phoenix (2000), who considered the same case.

## 3. Results

The mode I and mode II stress intensity factors obtained with the present variant of the DDDT are denoted by $K_I$ and $K_{II}$, respectively, while the corresponding stress intensity factors obtained with ABAQUS are denoted $K_{Iabq}$ and $K_{IIabq}$. The unit of the stress intensity factors is MPa$\sqrt{\text{mm}}$. For each order of the Jacobi polynomial expansion used, up to a maximum $N_p = 48$, the number of integration points was gradually increased until the maximum

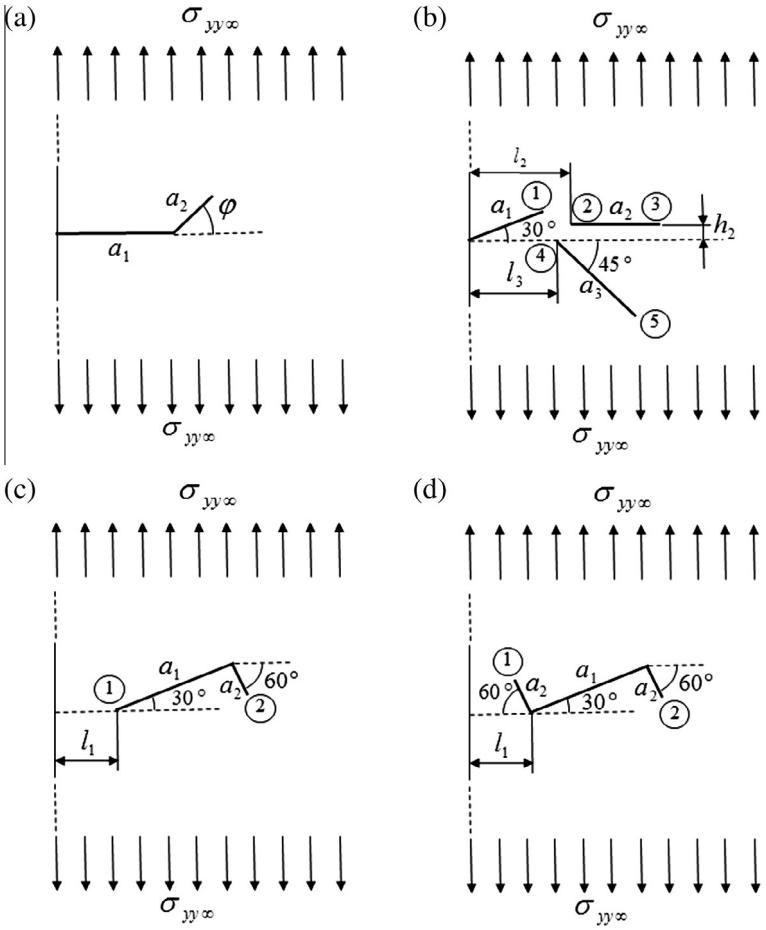


**Fig. 5.** Test cases (a) to (d).

absolute difference between consecutive calculations of the stress intensity factors was less than $1 \cdot 10^{-3}$. In the tables below the final number of integration points used is denoted by $M$. As a measure of the difference in the stress intensity factor solutions between the DDDT and ABAQUS the difference norm

$$d = \frac{\max\{|K_I - K_{Iabq}|, |K_{II} - K_{IIabq}|\}}{\sqrt{K_{Iabq}^2 + K_{IIabq}^2}} \tag{67}$$

was adopted and computed for each crack tip in the model. In situations involving several crack tips the maximum value of $d$ is reported as $d_{max}$.

The results for the single kinked edge crack (a) are shown in Tables 1–3. As seen in the tables the difference is limited to a maximum of 1% if the polynomial order $N_p = 6$. A difference of less than 0.5% could in all cases be achieved by increasing the polynomial order to $N_p = 16$, where the largest differences is encountered for the largest kink angle $\varphi = 80^\circ$. It is also observed that the accuracy, and the convergence rate with respect to increasing $N_p$, deteriorates as the ratio $a_2/a_1$ decreases. In case of $\varphi = 80^\circ$ with $a_2/a_1 = 0.1$ or $a_2/a_1 = 0.05$ not even $N_p = 48$ is enough to scale down $d_{max}$ below 0.1%. The logarithm of $d_{max}$ is plotted against every $N_p$ for all cases of the kinked edge crack considered in Fig. 8.

The results for the elastic half plane crosscut by one edge crack and two internal cracks (b) are reported in Table 4. It is obvious that straight cracks are less demanding from a numerical point of view than kinked (and/or branched) cracks. Very good agreement is reached already with $N_p = 6$ using relatively few integration points.

The results for the kinked internal crack (c), the doubly kinked internal crack (d), the branched crack (e), the kinked and branched internal crack (f), the doubly branched internal crack (g) and the branched internal crack with a weak singularity at the branch (h) are reported in Tables 5–10, respectively. Setting $N_p = 6$ assures in all these cases a difference to ABAQUS of less than 1%, while $N_p = 16$ gives a difference of less than 0.1%. Thus the analyses of the kinked and/or branched internal cracks perform somewhat better than the analyses of the kinked edge cracks. The logarithm of $d_{max}$ is plotted against every $N_p$ for the cases (b) to (h) in Fig. 9.

In 9 out of 16 cases the difference falls below 0.01% with an increasingly higher $N_p$. This is a remarkable small difference considering the fact that the comparison is made against another

**Table 1**
Results for the kinked edge crack, case (a), with $a_2/a_1 = 0.2$.

| $a_2/a_1$ | $\phi$ | $N_p$ | $M$ | $K_I$ | $K_{Iabq}$ | $K_{II}$ | $K_{IIabq}$ | $d_{max}$ |
|---|---|---|---|---|---|---|---|---|
| 0.2 | 30° | | | | 600.28 | | 195.51 | |
| | | 2 | 60 | 605.02 | | 198.53 | | $7.5 \cdot 10^{-3}$ |
| | | 6 | 120 | 599.92 | | 195.11 | | $6.3 \cdot 10^{-4}$ |
| | | 20 | 300 | 600.22 | | 195.47 | | $9.7 \cdot 10^{-5}$ |
| | | 48 | 700 | 600.28 | | 195.51 | | $2.2 \cdot 10^{-6}$ |
| 0.2 | 55° | | | | 425.89 | | 278.03 | |
| | | 3 | 80 | 421.43 | | 277.79 | | $8.8 \cdot 10^{-3}$ |
| | | 8 | 160 | 426.31 | | 277.80 | | $8.2 \cdot 10^{-4}$ |
| | | 48 | 800 | 425.94 | | 277.96 | | $1.4 \cdot 10^{-4}$ |
| 0.2 | 80° | | | | 229.45 | | 262.63 | |
| | | 4 | 120 | 232.44 | | 264.98 | | $8.6 \cdot 10^{-3}$ |
| | | 16 | 400 | 230.07 | | 262.42 | | $1.8 \cdot 10^{-3}$ |
| | | 32 | 700 | 229.74 | | 262.39 | | $8.4 \cdot 10^{-4}$ |
| | | 48 | 950 | 229.64 | | 262.37 | | $7.6 \cdot 10^{-4}$ |

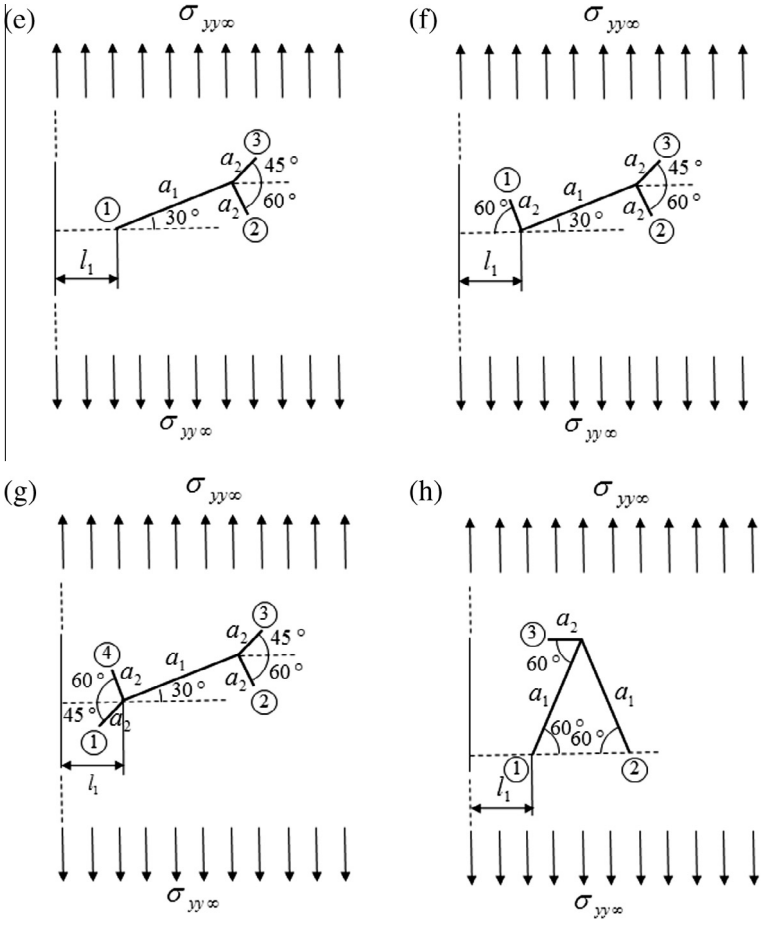


**Fig. 6.** Test cases (e) to (h).

**Table 2**
Results for the kinked edge crack, case (a), with $a_2/a_1 = 0.1$.

| $a_2/a_1$ | $\phi$ | $N_p$ | $M$ | $K_I$ | $K_{I\text{abq}}$ | $K_{II}$ | $K_{II\text{abq}}$ | $d_{max}$ |
|---|---|---|---|---|---|---|---|---|
| 0.1 | 30° | | | | 578.74 | | 183.59 | |
| | | 3 | 90 | 574.18 | | 185.02 | | $7.5 \cdot 10^{-3}$ |
| | | 10 | 240 | 578.24 | | 183.21 | | $8.3 \cdot 10^{-4}$ |
| | | 32 | 700 | 578.72 | | 183.56 | | $4.2 \cdot 10^{-5}$ |
| 0.1 | 55° | | | | 418.66 | | 264.77 | |
| | | 3 | 100 | 418.62 | | 266.67 | | $3.8 \cdot 10^{-3}$ |
| | | 6 | 180 | 418.83 | | 264.44 | | $6.8 \cdot 10^{-4}$ |
| | | 48 | 1200 | 418.75 | | 264.68 | | $1.8 \cdot 10^{-4}$ |
| 0.1 | 80° | | | | 235.67 | | 256.74 | |
| | | 4 | 160 | 238.28 | | 257.42 | | $7.5 \cdot 10^{-3}$ |
| | | 16 | 500 | 236.50 | | 255.94 | | $2.4 \cdot 10^{-3}$ |
| | | 48 | 1400 | 235.97 | | 256.19 | | $1.6 \cdot 10^{-3}$ |

**Table 3**
Results for the kinked edge crack, case (a), with $a_2/a_1 = 0.05$.

| $a_2/a_1$ | $\phi$ | $N_p$ | $M$ | $K_I$ | $K_{I\text{abq}}$ | $K_{II}$ | $K_{II\text{abq}}$ | $d_{max}$ |
|---|---|---|---|---|---|---|---|---|
| 0.05 | 30° | | | | 568.87 | | 174.82 | |
| | | 4 | 160 | 571.79 | | 179.22 | | $7.4 \cdot 10^{-3}$ |
| | | 16 | 550 | 568.29 | | 174.42 | | $9.7 \cdot 10^{-4}$ |
| | | 48 | 1400 | 568.82 | | 174.78 | | $7.7 \cdot 10^{-5}$ |
| 0.05 | 55° | | | | 418.70 | | 254.26 | |
| | | 5 | 220 | 419.40 | | 253.75 | | $1.4 \cdot 10^{-3}$ |
| | | 16 | 600 | 418.77 | | 253.57 | | $1.4 \cdot 10^{-3}$ |
| | | 24 | 850 | 418.80 | | 253.78 | | $9.7 \cdot 10^{-4}$ |
| | | 48 | 1600 | 418.80 | | 254.02 | | $4.9 \cdot 10^{-4}$ |
| 0.05 | 80° | | | | 245.51 | | 250.46 | |
| | | 6 | 280 | 247.48 | | 249.14 | | $5.6 \cdot 10^{-3}$ |
| | | 16 | 700 | 246.77 | | 249.06 | | $4.0 \cdot 10^{-3}$ |
| | | 48 | 1900 | 245.96 | | 249.78 | | $2.0 \cdot 10^{-3}$ |

approximate method (FEM) and not to analytic solutions. However, due to the slow convergence rate in some of the kinked edge crack cases, the largest difference to ABAQUS for $N_p = 48$ is still 0.2%. In 12 out of 16 cases $N_p = 16$ yields a difference less than 0.1%, with a maximum difference of 0.4% (for case (a) with $\varphi = 80°$ and $a_2/a_1 = 0.05$). Thus, there is generally not much to gain by increasing $N_p$ from 6 to 16, or even 48, since the difference in all cases is limited to 1% by choosing $N_p = 6$.

## 4. Discussion and conclusions

The main objective for the development of the technique is to enable efficient analysis of fatigue initiation and growth in steel and other metal alloys. For a single static analysis of a crack, or system of cracks, the efficiency is impaired by the fact that the evaluation of the hypersingular integrals is rather time consuming when using Jacobi polynomials to represent the dislocation dipole distribution. For repeated loading, however, the computation efficiency will improve, since the hypersingular integrals computed during the first loading cycle thenceforth could be reused in all subsequent loading cycles, provided of course that the end point singularities do not change as a result of branching or kinking of a crack segment. For such crack segments the hypersingular integrals needs to be recomputed. The hypersingular integrals must also be computed for any newly developed crack segments during the fatigue evolution. For fatigue analysis it is more important to

**Table 5**
Results for a kinked internal crack, case (c).

| Tip | ABAQUS results | | $N_p$ | 4 | 5 | 40 |
|---|---|---|---|---|---|---|
| | | | $M$ | 90 | 200 | 700 |
| 1 | $K_{I\text{abq}}$ | 341.93 | $K_I$ | 341.85 | 341.83 | 341.96 |
| | $K_{II\text{abq}}$ | 231.70 | $K_{II}$ | 231.62 | 231.68 | 231.69 |
| 2 | $K_{I\text{abq}}$ | 158.98 | $K_I$ | 159.11 | 159.09 | 159.00 |
| | $K_{II\text{abq}}$ | −227.04 | $K_{II}$ | −228.07 | −227.07 | −227.02 |
| | | | $d_{max}$ | $3.7 \cdot 10^{-3}$ | $3.9 \cdot 10^{-4}$ | $9.6 \cdot 10^{-5}$ |

**Table 6**
Results for a doubly kinked internal crack, case (d).

| Tip | ABAQUS results | | $N_p$ | 4 | 8 | 48 |
|---|---|---|---|---|---|---|
| | | | $M$ | 100 | 180 | 900 |
| 1 | $K_{I\text{abq}}$ | 219.95 | $K_I$ | 219.48 | 219.63 | 219.94 |
| | $K_{II\text{abq}}$ | −275.41 | $K_{II}$ | −276.52 | −275.10 | −275.39 |
| 2 | $K_{I\text{abq}}$ | 235.28 | $K_I$ | 234.90 | 234.98 | 235.29 |
| | $K_{II\text{abq}}$ | −236.15 | $K_{II}$ | −237.41 | −235.97 | −236.12 |
| | | | $d_{max}$ | $3.8 \cdot 10^{-3}$ | $9.2 \cdot 10^{-4}$ | $8.0 \cdot 10^{-5}$ |

**Table 7**
Results for a branched internal crack, case (e).

| Tip | ABAQUS results | | $N_p$ | 4 | 10 | 32 |
|---|---|---|---|---|---|---|
| | | | $M$ | 80 | 200 | 600 |
| 1 | $K_{I\text{abq}}$ | 375.62 | $K_I$ | 375.92 | 375.58 | 375.63 |
| | $K_{II\text{abq}}$ | 226.59 | $K_{II}$ | 226.16 | 226.64 | 226.61 |
| 2 | $K_{I\text{abq}}$ | 124.44 | $K_I$ | 123.68 | 124.53 | 124.45 |
| | $K_{II\text{abq}}$ | −165.46 | $K_{II}$ | −165.79 | −165.29 | −165.45 |
| 3 | $K_{I\text{abq}}$ | 261.81 | $K_I$ | 262.26 | 261.69 | 261.81 |
| | $K_{II\text{abq}}$ | 203.91 | $K_{II}$ | 203.54 | 203.89 | 203.91 |
| | | | $d_{max}$ | $3.7 \cdot 10^{-3}$ | $8.1 \cdot 10^{-4}$ | $4.7 \cdot 10^{-5}$ |

**Table 4**
Results for multiple edge and internal cracks, case (b).

| Tip | ABAQUS results | | $N_p$ | 3 | 4 | 6 |
|---|---|---|---|---|---|---|
| | | | $M$ | 50 | 60 | 70 |
| 1 | $K_{I\text{abq}}$ | 539.06 | $K_I$ | 537.81 | 539.13 | 539.08 |
| | $K_{II\text{abq}}$ | 161.95 | $K_{II}$ | 161.78 | 161.91 | 161.95 |
| 2 | $K_{I\text{abq}}$ | 304.19 | $K_I$ | 304.97 | 304.22 | 304.18 |
| | $K_{II\text{abq}}$ | −69.988 | $K_{II}$ | −69.058 | −69.712 | −69.996 |
| 3 | $K_{I\text{abq}}$ | 373.04 | $K_I$ | 373.11 | 373.05 | 373.05 |
| | $K_{II\text{abq}}$ | −49.236 | $K_{II}$ | −48.852 | −49.231 | −49.244 |
| 4 | $K_{I\text{abq}}$ | 248.40 | $K_I$ | 248.09 | 247.99 | 248.42 |
| | $K_{II\text{abq}}$ | −326.94 | $K_{II}$ | −325.64 | −326.79 | −326.96 |
| 5 | $K_{I\text{abq}}$ | 171.94 | $K_I$ | 171.39 | 171.91 | 171.94 |
| | $K_{II\text{abq}}$ | −194.17 | $K_{II}$ | −193.94 | −194.29 | −194.17 |
| | | | $d_{max}$ | $3.2 \cdot 10^{-3}$ | $9.9 \cdot 10^{-4}$ | $5.1 \cdot 10^{-5}$ |

**Table 8**
Results for a kinked and branched internal crack, case (f).

| Tip | ABAQUS results | | $N_p$ / $M$ | 4 / 100 | 6 / 140 | 16 / 350 | 48 / 900 |
|---|---|---|---|---|---|---|---|
| 1 | $K_{I\text{abq}}$ | 217.41 | $K_I$ | 215.76 | 218.31 | 217.48 | 217.40 |
| | $K_{II\text{abq}}$ | −287.55 | $K_{II}$ | −290.40 | −286.99 | −287.38 | −287.54 |
| 2 | $K_{I\text{abq}}$ | 197.12 | $K_I$ | 197.43 | 198.31 | 197.29 | 197.17 |
| | $K_{II\text{abq}}$ | −173.70 | $K_{II}$ | −171.66 | −172.32 | −173.51 | −173.68 |
| 3 | $K_{I\text{abq}}$ | 259.11 | $K_I$ | 258.68 | 257.94 | 258.93 | 259.08 |
| | $K_{II\text{abq}}$ | 243.33 | $K_{II}$ | 242.16 | 243.37 | 243.34 | 243.35 |
| | | | $d_{max}$ | $7.9 \cdot 10^{-3}$ | $5.3 \cdot 10^{-3}$ | $7.4 \cdot 10^{-4}$ | $1.8 \cdot 10^{-4}$ |

**Table 9**
Results for a doubly branched internal crack, case (g).

| Tip | ABAQUS results | | $N_p$ / $M$ | 6 / 140 | 16 / 300 | 48 / 900 |
|---|---|---|---|---|---|---|
| 1 | $K_{I\text{abq}}$ | 299.50 | $K_I$ | 298.12 | 299.39 | 299.49 |
| | $K_{II\text{abq}}$ | 295.98 | $K_{II}$ | 295.75 | 295.98 | 295.99 |
| 2 | $K_{I\text{abq}}$ | 188.99 | $K_I$ | 190.66 | 189.21 | 189.01 |
| | $K_{II\text{abq}}$ | −174.65 | $K_{II}$ | −175.21 | −174.71 | −174.66 |
| 3 | $K_{I\text{abq}}$ | 301.70 | $K_I$ | 299.46 | 301.40 | 301.68 |
| | $K_{II\text{abq}}$ | 229.17 | $K_{II}$ | 227.66 | 228.98 | 229.16 |
| 4 | $K_{I\text{abq}}$ | 162.30 | $K_I$ | 163.38 | 162.44 | 162.31 |
| | $K_{II\text{abq}}$ | −205.34 | $K_{II}$ | −204.78 | −205.27 | −205.33 |
| | | | $d_{max}$ | $6.5 \cdot 10^{-3}$ | $8.6 \cdot 10^{-4}$ | $7.7 \cdot 10^{-5}$ |

**Table 11**
Case (f) analysed by treating weakly singular end points as regular.

| Tip | ABAQUS results | | $N_p$ / $M$ | 6 / 140 | 16 / 300 | 48 / 900 |
|---|---|---|---|---|---|---|
| 1 | $K_{I\text{abq}}$ | 217.41 | $K_I$ | 187.31 | 214.04 | 217.14 |
| | $K_{II\text{abq}}$ | −287.55 | $K_{II}$ | −291.83 | −287.77 | −287.55 |
| 2 | $K_{I\text{abq}}$ | 197.12 | $K_I$ | 118.77 | 187.46 | 196.24 |
| | $K_{II\text{abq}}$ | −173.70 | $K_{II}$ | −165.48 | −170.10 | −172.81 |
| 3 | $K_{I\text{abq}}$ | 259.11 | $K_I$ | 325.00 | 268.55 | 260.19 |
| | $K_{II\text{abq}}$ | 243.33 | $K_{II}$ | 310.77 | 254.45 | 244.88 |
| | | | $d_{max}$ | 0.30 | $3.7 \cdot 10^{-2}$ | $4.4 \cdot 10^{-3}$ |

receive high accuracy with a minimum number of polynomials needed to represent the dipole density distribution, and to reduce the number of integration points associated with regular integration, than to enable fast calculation of the singular integrals.

Test cases involving single or multiple straight, kinked and/or branched cracks have been analysed to assure that the theory and implementation works for crack segments with different end point behaviours. The results indicate that Jacobi polynomial expansions of order $N_p = 6$ gives an accuracy to within 1% and that $N_p = 16$ reduces the error to a few tenth of a percent. For the kinked edge crack it is found that the convergence towards minor descrepancies, when using higher $N_p$, is slow when the kink angle is large and the kink length is small (see Fig. 8). This may be due to that the asymmetric part of the deformation at the kink in this case is large relative to the symmetric part. Since the singular behaviour, as a whole, in this analysis is governed by the symmetric singularity at the kink, the influence of the inaccurately represented asymmetric part may become prominent in these cases, leading to the need for a very large $N_p$ to compensate for this deficiency. Nevertheless, this fact does not seem to affect the efficiency of the method when it comes to compute stress intensity factors accurate to within 1%. For most engineering, and even scientific, purposes an accuracy of 1% should be sufficient considering all other uncertainties involved in the analysis. Also, The fact that the present code operates in 2D brings about a considerably larger error than 1%, as compared to the 3D reality. 3D analyses of notched and cracked plates subjected to asymmetric loading reveals that mode II also generates a coupled out-of-plane singular mode which varies through the thickness of the plate (cf. Berto et al., 2011). Such effects, along with other 3D effects, are clearly not taken into account in a 2D analysis of the problem like the one considered here.

The number of integration points needed increases with the order of the Jacobi polynomial expansion used in the analysis. For $N_p = 6$ the number $M = 300$ should be sufficient, while $N_p = 16$ requires many more points, lets say $M = 700$, based on the results presented above. In any case there is a substantial size reduction compared to the FEM. In case (f), for instance, the FEM model contains 65544 DOF's, while $N_p = 6$, $N_p = 16$ and $N_p = 48$ contains 60, 140 and 396 unknown coefficients, respectively.

Due to the fact that some analysts, *e.g.* Denda and Dong (1999), claim that good results could be obtained by disregarding weak end point singularities and instead treat them as regular, the impact of this simplification was explored. This means that the second and third terms of Eq. (33) are not used, *i.e.* $\gamma_+$ and $\gamma_-$ are set to either 1/2 (for a crack tip end point) or 0 (for all other end points). By doing so, and again considering case (f), the results according to Table 11 are obtained.

**Table 10**
Results for a branched internal crack with a weak singularity at the branch, case (h).

| Tip | ABAQUS results | | $N_p$ / $M$ | 5 / 180 | 16 / 500 | 48 / 1400 |
|---|---|---|---|---|---|---|
| 1 | $K_{I\text{abq}}$ | 97.785 | $K_I$ | 97.493 | 97.782 | 97.776 |
| | $K_{II\text{abq}}$ | 274.63 | $K_{II}$ | 274.96 | 274.67 | 274.63 |
| 2 | $K_{I\text{abq}}$ | 129.06 | $K_I$ | 129.09 | 129.03 | 129.06 |
| | $K_{II\text{abq}}$ | −272.74 | $K_{II}$ | −272.47 | −272.77 | −272.75 |
| 3 | $K_{I\text{abq}}$ | 212.81 | $K_I$ | 212.52 | 212.64 | 212.81 |
| | $K_{II\text{abq}}$ | 11.804 | $K_{II}$ | 11.810 | 11.954 | 11.821 |
| | | | $d_{max}$ | $1.4 \cdot 10^{-3}$ | $8.2 \cdot 10^{-4}$ | $7.7 \cdot 10^{-5}$ |

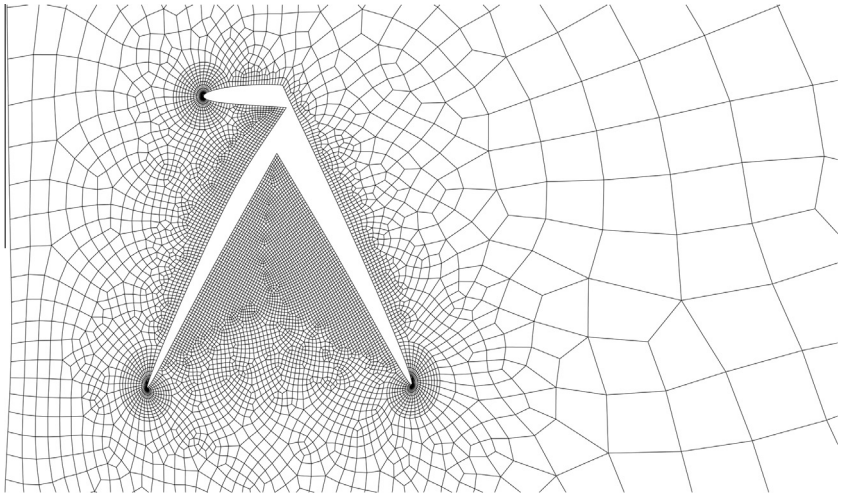

**Fig. 7.** Close up of FE-mesh for test case (h) shown in the deformed state.

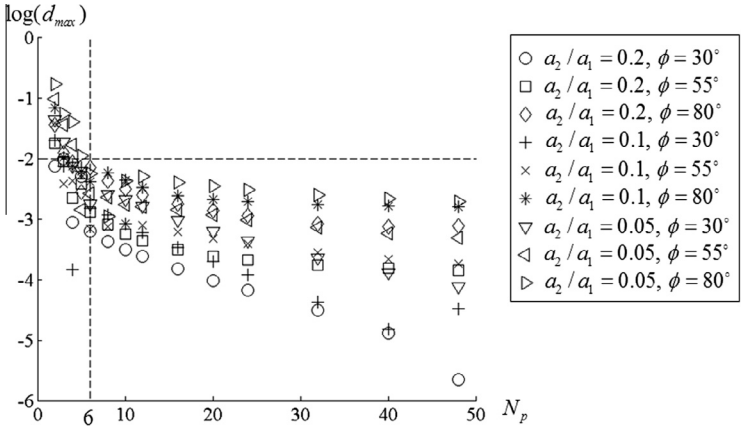


**Fig. 8.** $\log(d_{max})$ versus $N_p$ for the kinked edge crack, case (a).

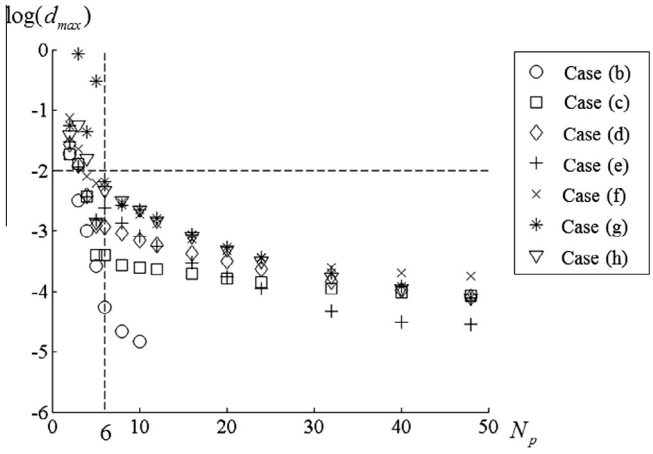


**Fig. 9.** $\log(d_{max})$ versus $N_p$ for case (b) to case (h).

From this table it is seen that $N_p = 6$ gives results that are completely useless, and that a $N_p$ as high as 48 is required to obtain results just slightly better than those obtained with $N_p = 6$ when taking weakly singular end point behaviours into account in the dipole density representation. Good results could hence be obtained, albeit at the expense of a vast increase in the number of unknown coefficients, from 60 to 392, with an accompanying increase in computation time. The incorporation of end point singularities in the dipole density representation thus increases the efficiency of the calculation. The only drawback seems to be that it makes the theoretical outline and implementation more spacious. In cases not possessing any weakly singular end points it does not matter which version of the method to use. Applying the simplified version of the method to *e.g.* case (g), yields the same result as in Table 9.

It is believed that the method could be further improved if the correct singular asymptotic behaviours for the symmetric and asymmetric parts at crack kinking/branching could be accounted for in the representation for the dislocation dipole density. This would presumably improve the convergence rate in cases where crack kinks/branches are dominated by asymmetric loading. Moreover, it would also enable the determination of stress intensities at crack kinking/branching. In order to study crack closure contact constraints has to be enforced that prevents interpenetration of the crack surfaces. Both these aspects are left for future research.

## Acknowledgements

The research presented in this report has been partly sponsored by the Swedish KK-foundation. The authors are grateful for this support.

## Appendix A. Transformation relations

In practice it is convenient to express the transformation relation in Eq. (16) in a slightly different form. If the influence coefficients are stored in vectors the relation between the transformed influence coefficients and the influence coefficients expressed in the global coordinate system becomes

$$L = \begin{bmatrix} L_{22(p)}^{22(q)} \\ L_{22(p)}^{12(q)} \\ L_{21(p)}^{22(q)} \\ L_{21(p)}^{12(q)} \end{bmatrix} = \mathbf{A} \begin{bmatrix} L_{11}^{11} \\ L_{11}^{22} \\ L_{11}^{12} \\ L_{22}^{11} \\ L_{22}^{22} \\ L_{22}^{12} \\ L_{12}^{11} \\ L_{12}^{22} \\ L_{12}^{12} \end{bmatrix} \tag{A.1}$$

where $\mathbf{A}$ is a 4 by 9 transformation matrix given by

$$\mathbf{A} = \begin{bmatrix} \sin\theta_p \sin^2\theta_q & \cos^2\theta_q \sin^2\theta_p & \cdots \\ -\cos\theta_q \sin^2\theta_p \sin\theta_q & \cos\theta_q \sin^2\theta_p \sin\theta_q & \\ -\cos\theta_p \sin\theta_p \sin^2\theta_q & -\cos\theta_p \cos^2\theta_q \sin\theta_p & \\ \cos\theta_p \cos\theta_q \sin\theta_p \sin\theta_q & -\cos\theta_p \cos\theta_q \sin\theta_p \sin\theta_q & \end{bmatrix}$$

$$\begin{bmatrix} -2\cos\theta_q \sin^2\theta_p \sin\theta_q & \cos^2\theta_p \sin^2\theta_q & \cdots \\ \sin^2\theta_p\left(\cos^2\theta_q - \sin^2\theta_q\right) & -\cos^2\theta_p \cos\theta_q \sin\theta_q & \\ 2\cos\theta_p \cos\theta_q \sin\theta_p \sin\theta_q & \cos\theta_p \sin\theta_p \sin^2\theta_q & \\ -\cos\theta_p \sin\theta_p\left(\cos^2\theta_q - \sin^2\theta_q\right) & -\cos\theta_p \cos\theta_q \sin\theta_p \sin\theta_q & \end{bmatrix}$$

$$\begin{bmatrix} \cos^2\theta_p \cos^2\theta_q & -2\cos^2\theta_p \cos\theta_q \sin\theta_q & \cdots \\ \cos^2\theta_p \cos\theta_q \sin\theta_q & \cos^2\theta_p\left(\cos^2\theta_q - \sin^2\theta_q\right) & \\ \cos\theta_p \cos^2\theta_q \sin\theta_p & -2\cos\theta_p \cos\theta_q \sin\theta_p \sin\theta_q & \\ \cos\theta_p \cos\theta_q \sin\theta_p \sin\theta_q & \cos\theta_p \sin\theta_p\left(\cos^2\theta_q - \sin^2\theta_q\right) & \end{bmatrix}$$

$$\begin{bmatrix} -\sin(2\theta_p) \sin^2\theta_q & -\sin(2\theta_p) \cos^2\theta_q & \cdots \\ \sin(2\theta_p) \cos\theta_q \sin\theta_q & -\sin(2\theta_p) \cos\theta_q \sin\theta_q & \\ \cos(2\theta_p) \sin^2\theta_q & \cos(2\theta_p) \cos^2\theta_q & \\ -\cos(2\theta_p) \cos\theta_q \sin\theta_q & \cos(2\theta_p) \cos\theta_q \sin\theta_q & \end{bmatrix}$$

$$\begin{bmatrix} 2\sin(2\theta_p) \cos\theta_q \sin\theta_q \\ -\sin(2\theta_p)\left(\cos^2\theta_q - \sin^2\theta_q\right) \\ -2\cos(2\theta_p) \cos\theta_q \sin\theta_q \\ \cos(2\theta_p)\left(\cos^2\theta_q - \sin^2\theta_q\right) \end{bmatrix} \tag{A.2}$$

The transformation of the influence coefficients associated with stress computation at an arbitrary field point given by Eq. (65), could be expressed as

$$\begin{bmatrix} L_{ij}^{22(q)} \\ L_{ij}^{12(q)} \end{bmatrix} = \mathbf{B} \begin{bmatrix} L_{ij}^{11} \\ L_{ij}^{22} \\ L_{ij}^{12} \end{bmatrix} \tag{A.3}$$

where $ij = 11, 22, 12$. The transformation matrix $\mathbf{B}$ could be derived as

$$\mathbf{B} = \begin{bmatrix} \sin^2\theta_q & \cos^2\theta_q & -2\cos\theta_q \sin\theta_q \\ -\cos\theta_q \sin\theta_q & \cos\theta_q \sin\theta_q & \cos^2\theta_q - \sin^2\theta_q \end{bmatrix} \tag{A.4}$$

## References


Bathias, C., 1999. There is no infinite fatigue life in metallic materials. Fatigue Fract. Eng. Mater. Struct. 22, 559–565.

Berto, F., Lazzarin, P., Kotousov, A., Harding, S., 2011. Out-of-plane singular stress fields in V-notched plates and welded lap joints induced by in-plane shear load conditions. Fatigue Fract. Eng. Mater. Struct. 34, 291–304.

Bilby, B.A., Eshelby, J.D., 1968. Dislocations and the theory of fracture. In: Liebowitz, H. (Ed.), Fracture, An Advanced Treatise, vol. 1. Academic Press, New York, pp. 99–182.

Bueckner, H., 1958. The propagation of cracks and the energy of elastic deformation. Trans. Am. Soc. Mech. Eng. 80, 1225–1230.

Burton, J.K., Phoenix, S.L., 2000. Superposition method for calculating singular stress fields at kinks, branches and tips in multiple crack arrays. Int. J. Fract. 102, 99–139.

Crouch, S.L., 1976. Solution of plane elasticity problems by the displacement discontinuity method. Int. J. Numer. Methods Eng. 10, 301–343.

Cruse, T.A., 1988. Boundary Element Analysis in Computational Fracture Mechanics. Kluwer Academic Publishers.

Dai, D.N., 2002. Modelling cracks in finite bodies by distributed dislocation dipoles. Fatigue Fract. Eng. Mater. Struct. 25, 27–39.

Denda, M., Dong, Y.F., 1999. Analytical formulas for a 2-D crack tip singular boundary element for rectilinear cracks and crack growth analysis. Eng. Anal. Boundary Elem. 23, 35–49.

Hills, D.A., Kelly, P.A., Dai, D.N., Korsunsky, A.M., 1996. Solution of Crack Problems-The distributed Dislocation Technique. Kluwer Academic Publishers, Dordrecht, The Netherlands.

Kaya, A.C., Erdogan, F., 1987. On the solution of integral equations with strongly singular kernels. Q. Appl. Math. XLV (1), 105–122.

Korsunsky, A.M., Hills, D.A., 1995. The solution of plane crack problems by dislocation dipole procedures. J. Strain Anal. 30 (1), 21–27.

Marji, M.F., Dehghani, I., 2010. Kinked crack analysis by hybridized boundary element/boundary collocation method. Int. J. Solids Struct. 47, 922–933.

Mi, Y., 1996. Three-dimensional analysis of crack growth. In: Brebbia, C.A., Connor, J. (Eds.), Topics in Engineering, vol. 28. Computational Mechanics Publications.

Portela, A., Aliabadi, H., Rooke, D.P., 1992. The dual boundary element method: effective implementation for crack problems. Int. J. Numer. Methods Eng. 33 (6), 1269–1287.

Shou, K.J., Crouch, S.L., 1995. A higher order displacement discontinuity method for analysis of crack problems. Int. J. Rock Mech. Min. Sci. Geomech. Abstracts 32 (1), 49–55.

Wang, Y.B., Chau, K.T., 1997. A new boundary element for plane elastic problems involving cracks and holes. Int. J. Fract. 87, 1–20.

Williams, M.L., 1952. Stress singularities resulting from various boundary conditions in angular corners of plates in extension. J. Appl. Mech. 19, 526–528.

Yavuz, A.K., Phoenix, S.L., TerMaath, S.C., 2006. An accurate and fast analysis for strongly interacting multiple crack configurations including kinked (V) and branched (Y) cracks. Int. J. Solids Struct. 43, 6727–6750.

Yingzhi, L., Hills, D.A., 1990. Stress intensity factor solutions for kinked surface cracks. Int. J. Numer. Methods Eng. 25, 21–27.

Zang, W.L., Gudmundson, P., 1988. A boundary integral method for internal piecewise smooth crack problems. Int. J. Fract. 38, 275–294.